63p.

NASA TM X-53008

THEORETICAL AND EXPERIMENTAL INVESTIGATION OF BOUNDARY LAYER CONTROL IN LOW-DENSITY NOZZLES BY WALL SUCTION AND COOLING

by M. R. BOTTORFF AND K. W. ROGERS*
Aero-Astrodynamics Laboratory

*Engineering Center
 University of Southern California

NASA

George C. Marshall
Space Flight Center,
Huntsville, Alabama

THEORETICAL AND EXPERIMENTAL INVESTIGATION OF BOUNDARY LAYER CONTROL IN LOW-DENSITY NOZZLES BY WALL SUCTION AND COOLING

By

M. R. Bottorff and K. W. Rogers[*]

George C. Marshall Space Flight Center
Huntsville, Alabama

ABSTRACT

This report presents the results of a theoretical and experimental investigation on the reduction of boundary layer thickness in low-density nozzles by wall cooling, wall suction, and a combination of these two. Potentially there is a twofold benefit in reducing the thickness of the nozzle boundary layer: (1) a possible increase in diffuser effectiveness, and (2) a possible reduction in the amount of boundary layer flow for a specified usable test section size, or an increase in the size of the usable test section for a given nozzle mass flow. The theoretical development starts with the proper integral relationship for a compressible laminar boundary layer. The normal velocity at the wall is allowed to be finite to include the effects of wall suction. Definitions of momentum and displacement thicknesses which account for transverse curvature are used. The results of Iglisch, who developed an exact solution for incompressible flat plate flow with suction, are used to estimate skin friction coefficients. The Prandtl number is assumed to be unity, and two-dimensional values of δ^*/θ are used. An exponential velocity profile which takes wall suction into account was used to estimate boundary layer height.

The theoretical results were checked by an experiment in which a Mach number 9 - to - 11 porous nozzle was operated at unit Reynolds numbers in the range of 100/inch to 600/inch. Pitot pressure surveys were used to determine the exit Mach number and boundary layer thickness. Theoretical Mach number predictions are shown to agree with the experimental results to within 5%, and boundary layer height predictions to within 10%.

Theoretical results are presented which show the effects of suction and wall cooling at several Reynolds numbers on nozzle diameter and uniform core size for a given throat area and Mach number distribution. It is concluded that the use of suction and cooling may result in a larger test section size, but that the merits of a cooled porous wall in any specific case must be decided from an analysis of the complete wind tunnel system.

[*]Engineering Center, University of Southern California

NASA-GEORGE C. MARSHALL SPACE FLIGHT CENTER

NASA-GEORGE C. MARSHALL SPACE FLIGHT CENTER

TECHNICAL MEMORANDUM X-53008

THEORETICAL AND EXPERIMENTAL INVESTIGATION OF BOUNDARY
LAYER CONTROL IN LOW-DENSITY NOZZLES BY
WALL SUCTION AND COOLING

By

M. R. Bottorff and K. W. Rogers [*]

[*]Engineering Center
University of Southern California

AERODYNAMICS DIVISION
AERO-ASTRODYNAMICS LABORATORY

TABLE OF CONTENTS

LIST OF ILLUSTRATIONS

LIST OF ILLUSTRATIONS (Cont'd)

DEFINITION OF SYMBOLS

Symbol	Definition
a	nozzle wall radius
A	area
C_f	local skin friction coefficient
D	diameter of suction hole
h	enthalpy per unit mass
L	nozzle wall thickness
$\dot{m}$	mass flow rate
n	pressure gradient parameter
P	pressure
P_T	stagnation pressure
P_T'	stagnation pressure behind normal shock
Pr	Prandtl number
Re	Reynolds number
T	temperature
T_T	stagnation temperature
u	velocity
v_0	uniform suction velocity
$\dot{w}$	weight flow rate
x, y, r, s	nozzle coordinates (see Figure 3)
γ	ratio of specific heats
δ	boundary layer thickness

DEFINITION OF SYMBOLS (Cont'd)

Symbol	Definition
δ^*	boundary layer displacement thickness
θ	boundary layer momentum thickness
μ	viscosity
ξ	$(v_0/u_1)^2 \, Re_1$
ρ	density
ϕ	ratio of open area to total wall area
ϕ'	ratio of effective open area to total wall area
ω	nozzle wall half-angle

SUBSCRIPTS

o	wall
1	freestream
*	sonic condition
aw	adiabatic wall
ec	expansion core
s	suction

THEORETICAL AND EXPERIMENTAL INVESTIGATION OF BOUNDARY LAYER CONTROL IN LOW-DENSITY NOZZLES BY WALL SUCTION AND COOLING

By

M. R. Bottorff and K. W. Rogers[*]

SUMMARY

This report presents the results of a theoretical and experimental investigation on the reduction of boundary layer thickness in low-density nozzles by wall cooling, wall suction, and a combination of these two. Potentially there is a twofold benefit in reducing the thickness of the nozzle boundary layer: (1) a possible increase in diffuser effectiveness, and (2) a possible reduction in the amount of boundary layer flow for a specified usable test section size, or an increase in the size of the usable test section for a given nozzle mass flow. The theoretical development starts with the proper integral relationship for a compressible laminar boundary layer. The normal velocity at the wall is allowed to be finite to include the effects of wall suction. Definitions of momentum and displacement thicknesses which account for transverse curvature are used. The results of Iglisch, who developed an exact solution for incompressible flat plate flow with suction, are used to estimate skin friction coefficients. The Prandtl number is assumed to be unity, and two-dimensional values of δ^*/θ are used. An exponential velocity profile which takes wall suction into account was used to estimate boundary layer height.

The theoretical results were checked by an experiment in which a Mach number 9 - to - 11 porous nozzle was operated at unit Reynolds numbers in the range of 100/inch to 600/inch. Pitot pressure surveys were used to determine the exit Mach number and boundary layer thickness. Theoretical Mach number predictions are shown to agree with the experimental results to within 5%, and boundary layer height predictions to within 10%.

---

[*]Engineering Center, University of Southern California

Theoretical results are presented which show the effects of suction and wall cooling at several Reynolds numbers on nozzle diameter and uniform core size for a given throat area and Mach number distribution. It is concluded that the use of suction and cooling may result in a larger test section size, but that the merits of a cooled porous wall in any specific case must be decided from an analysis of the complete wind tunnel system.

I. INTRODUCTION

One of the main problems in designing a hypersonic low-density wind tunnel is devising a pumping system that will handle the high volume flows at the tunnel exit. These high volume flows result primarily from the low pressure recovery associated with a diffuser operating with an entering flow field that is largely composed of boundary layer. A secondary cause of the high volume flow is the direct effect of the thick boundary layer in the nozzle. Since the boundary layer flow sometimes fills a large part of the nozzle, it is necessary in such instances to have a nozzle diameter many times that of the usable test section. This flow in the boundary layer must still be pumped, and it contributes significantly to the high volume flow. Thus, it appears that potentially there is a twofold benefit in reducing the thickness of the nozzle boundary layer: (1) a possible increase in diffuser effectiveness, and (2) a reduction in the amount of boundary layer flow that must be pumped for a specified test section size, or an increase in the size of the uniform test section for a given mass flow.

This report presents the results of a theoretical and experimental study in the control o_ boundary layers in low-density wind tunnel nozzles. The work was carried out by the University of Southern California Engineering Center under National Aeronautics and Space Administration Contract NAS 8-5056. The NASA Marshall Space Flight Center, Huntsville, Alabama, instituted the contract in an attempt to develop an understanding of nozzle boundary layer control which would be useful in the design of nozzles for a low density test facility. The facility is to be of the cryopumped type (one-kilowatt refrigerator capacity), wherein the flow leaving the nozzle is condensed on an array of cold plates. The planned Mach number range is from 3 to 12. The maximum nozzle flow rate which can be continually accepted by a 1-KW cryopump is about 2.8 grams of nitrogen per second (this assumes that all the flow has been precooled to 100°K). Thus, although the boundary layer study herein described uses a general approach, the above considerations served more or less as guidelines, and the experimental portion of the study was performed in a small cryopumped tank. This tank closely simulated the conditions which should be encountered in the full scale facility.

II. FACTORS AFFECTING NOZZLE BOUNDARY LAYER CONTROL

For the purposes of this study, the "control" of the boundary layer means reducing the height and preventing separation. For a fixed Reynolds number, the parameters having the greatest effect on the boundary layer height are (1) pressure gradient, (2) surface roughness, (3) ratio of surface temperature to freestream temperature, and (4) surface suction or injection. These parameters are discussed in the following sections.

A. Pressure Gradient

In a nozzle, the pressure gradient is favorable (i.e., negative), and increasing the pressure gradient will generally reduce the nozzle length and lower the boundary layer height in the test section. However, since the magnitude of this gradient depends upon the Mach number gradient, and large test section Mach number gradients are undesirable, there is a limit to the allowable pressure gradient. If the nozzle is to have a region of uniform parallel flow, there is a minimum nozzle length required; however, Reference 1 shows that the nozzle length can be significantly reduced if small Mach number gradients are acceptable.

B. Surface Roughness

Surface roughness has the potential of influencing the boundary layer height in two regimes.

On the macroscopic scale, reducing the surface roughness will retard the transition to turbulent flow when the roughness elements are greater than some critical value. When the roughness elements are below this value, additional smoothing of the surface has no effect on the transition, and apparently the laminar boundary layer is unchanged also. With ordinary care the roughness of machined surfaces is below the critical value.

On the microscopic scale, Reference 2 shows that surfaces are attainable where a significant fraction of the rebounding molecules have their tangential momentum unchanged. In the limiting case with no loss of tangential momentum at the surface, the boundary layer could be eliminated; unfortunately, the techniques required to produce these surfaces are not suitable for wind tunnel construction, and the use of surfaces of this degree of smoothness does not seem feasible.

C. Temperature Ratio

Reducing the wall temperature causes a reduction in boundary layer height. For example, Reference 3 shows that reducing the wall temperature from adiabatic wall temperature to freestream temperature reduces a two-dimensional laminar boundary layer by 50% at M = 7.0. The reduction is somewhat greater at the higher Mach numbers. Thus, a cooled nozzle wall appears to be a useful means of reducing the boundary layer height. This wall cooling also has structural advantages, since at high Mach numbers the adiabatic wall temperature is too high for most materials.

D. Surface Suction and Injection

There have been many papers published on the use of surface injection to reduce wall heat transfer, but the use of this process causes an increase in the boundary layer height. Reference 4 shows that the converse is true, that suction increases the heat transfer and reduces the boundary layer height. Stalder [5] describes the performance of a Mach number 4 porous nozzle developed at the University of California Low-Density Facility. This nozzle was constructed by bolting together a series of flat plates, machining the desired contour, and then removing every other plate to achieve the desired porosity. It was found that by varying the plate back pressure, the Mach number could be kept nearly constant over a wide Reynolds number range.

To demonstrate the possibilities of suction and to present the overall trends, calculations were made on the reduction in boundary layer height that can be attained using suction and cold walls on a flat plate in a uniform stream. The computations used the equations of Reference 6 (summarized in Appendix A) and were made for a freestream Mach number of 10 with a unit Reynolds number of 600/in and suction velocity of 2.26% of the freestream velocity. These conditions are roughly those which one would obtain at a flow rate of 1 gram/sec in a 12-inch diameter nozzle with a displacement thickness of 2.8 inches. The suction velocity is approximately that resulting from a 50%-open-area plate. The results of the calculations are presented in Figure 1. It is apparent that the cooling reduces the boundary layer height by a fixed fraction as the plate length is increased, whereas the suction causes an increasing fractional reduction as the plate length is increased. Thus the cooling produces another "similar" solution while the suction does not. The effect of the suction can be roughly visualized as imposing a uniform normal velocity on the flow over the plate. Since this imposed velocity is small compared to the freestream velocity, the boundary layer height is practically unaffected where the growth rate of the boundary layer is comparable to the freestream velocity, i.e., at the front of the plate. Aft on the plate, the boundary layer growth rate diminishes and

the imposed suction velocity is increasingly effective in reducing the height. This model is useful only for explaining the major trends and does not quantitatively represent the problem, however.

For comparison, the boundary layer height has been calculated for a unit Reynolds number of 200/inch, while holding the other factors fixed. The two cold-wall calculations are compared in Figure 2. Here it is seen that for a fixed longitudinal location, the fractional reduction in boundary layer height is smaller for the lower unit Reynolds number case. This illustrates a possible difficulty in using this boundary layer control technique at extremely low unit Reynolds numbers.

E. Combined Suction and Cooling in a Cryopumped Wind Tunnel

In a conventional low-density wind tunnel, the feasibility of reducing the boundary layer height by means of suction is limited by the very large suction volume flow which must be pumped. In fact, an analysis by Enkenhus [7] demonstrated that the beneficial effect of suction on reducing the boundary layer height and increasing the test core size could be just as well accomplished by adding the suction pumps to the main test section flow pumps and increasing the nozzle size.

There is one pump, however, which can overcome many of the problems associated with high volume flows. This is the cryopump, which uses a highly cooled surface to condense the tunnel flow. In a typical installation using a helium refrigerator, extremely low pressures (of the order of 10^{-6} mm Hg or lower) are available if the tunnel gas is nitrogen or a combination of nitrogen and oxygen. These pressures are much lower than the static pressures of a typical low density facility, so it is possible to place the condenser plates in a chamber downstream of the test section and thus provide the low pressure region required to operate the tunnel.

Rogers [8] has investigated the possibilities of boundary layer control in a small-scale wind tunnel of this type. It is shown in Reference 8 that the use of suction combined with highly cooled nozzle walls (liquid nitrogen was used in this case) results in a lower heat load to the cryopump, so that larger tunnel mass flows may be accepted. Thus, the use of wall suction and cooling in a cryopumped wind tunnel appears to be an especially promising means of reducing the height of the boundary layer and increasing the size of the test core. The effects of combined suction and cooling are examined quantitatively in Section VI of this report.

III. THEORETICAL DEVELOPMENT

A literature search was made for methods of computing the thickness of a laminar low-density boundary layer in an axisymmetric nozzle. The search yielded three approximate methods for boundary layer calculation, namely, those of Durand and Potter [9], Johnson [10], and Maslach and Sherman [11].

Of the above references, only the first takes into account transverse curvature effects in defining displacement thickness (δ^*) and momentum thickness (θ). The effect of transverse curvature on axisymmetric boundary layers is discussed by Probstein and Elliott [12]. This effect is important if the boundary layer thickness comprises a significant fraction of the nozzle radius, which is the case in a low density nozzle. The following development therefore parallels the work of Durand and Potter [9]. Changes have been made where necessary to include the effects of wall suction. The coordinate system is given in Figure 3, where the expression "expansion core" has been retained from Durand and Potter. This "core" is the one to which δ^* is added to obtain the wall contour, but in the case of suction it does not determine the area ratio of the nozzle, since some of the flow has "expanded" through the walls.

A. Boundary Layer Momentum Integral for Computation of δ^*

We begin with the continuity and momentum equations for axially symmetric flow.

Continuity:

$$\frac{\partial}{\partial s} (\rho u r) + \frac{\partial}{\partial y} (\rho v r) = 0. \tag{1}$$

Momentum:

$$\rho u \frac{\partial u}{\partial s} + \rho v \frac{\partial u}{\partial y} = - \frac{dp}{ds} + \frac{\partial}{\partial y} \left(\mu \frac{\partial u}{\partial y} \right) + \frac{\mu}{r} \frac{\partial r}{\partial y} \frac{\partial u}{\partial y} . \tag{2}$$

Multiplying equation (2) by r and integrating through the boundary layer from 0 to δ gives

$$\int_0^\delta \rho u r \frac{\partial u}{\partial s} dy + \int_0^\delta \rho v r \frac{\partial u}{\partial y} dy = - \int_0^\delta r \frac{dp}{ds} dy + \int_0^\delta r \frac{\partial}{\partial y} \left(\mu \frac{\partial u}{\partial y} \right) dy$$

$$+ \int_0^\delta \mu \frac{\partial u}{\partial y} \frac{\partial r}{\partial y} dy. \tag{3}$$

6

Now if the continuity equation is integrated with suction allowed at the wall ($v_o \neq 0$), it becomes

$$\rho v r - \rho_o v_o a = - \int_0^y \frac{\partial}{\partial s} \rho u r \, dy. \qquad (4)$$

Substituting equation (4) into equation (3), we have

$$\int_0^\delta \rho u r \frac{\partial u}{\partial s} \, dy - \int_0^\delta \frac{\partial u}{\partial y} \left[\int_0^y \frac{\partial}{\partial s} \rho u r \, dy \right] dy + \int_0^\delta \frac{\partial u}{\partial y} \rho_o v_o a \, dy$$

$$= - \int_0^\delta r \frac{dp}{ds} \, dy + \int_0^\delta r \frac{\partial}{\partial y} \left(\mu \frac{\partial u}{\partial y} \right) dy + \int_0^\delta \mu \frac{\partial u}{\partial y} \frac{\partial r}{\partial y} \, dy. \qquad (5)$$

Integrating by parts the second term on the left hand side and the third term on the right hand side, and rearranging, we obtain

$$\int_0^\delta \frac{\partial}{\partial s} \rho u^2 r \, dy - u_1 \int_0^\delta \frac{\partial}{\partial s} \rho u r \, dy = - \frac{dp}{ds} \int_0^\delta r \, dy - a \, \mu_o \left(\frac{\partial u}{\partial y} \right)_o$$

$$- \int_0^\delta \frac{\partial u}{\partial y} \rho_o v_o a \, dy. \qquad (6)$$

If we substitute Euler's equation $- dp/ds = \rho_1 u_1 \frac{\partial u_1}{\partial s}$ for the pressure gradient, and integrate the last term of equation (6), we have (after multiplying by -1)

$$- \int_0^\delta \frac{\partial}{\partial s} \rho r u^2 \, dy + u_1 \int_0^\delta \frac{\partial}{\partial s} \rho u r \, dy + \rho_1 \, u_1 \frac{\partial u}{\partial s} \int_0^\delta r \, dy = a \, \mu_o \left(\frac{\partial u}{\partial y} \right) + u_1 \rho_o v_o a.$$

$$(7)$$

7

If the indicated differentiation in the first two terms is carried out, and the term

$$\int_0^\delta \rho r u \frac{\partial u_1}{\partial s} \, dy$$

is added to and subtracted from equation (7), we get

$$\int_0^\delta \frac{\partial}{\partial s} \left[\rho r (u u_1 - u^2) \right] \, dy - \int_0^\delta \rho r u \frac{\partial u_1}{\partial s} \, dy + \rho_1 u_1 \frac{\partial u_1}{\partial s} \int_0^\delta r \, dy$$

$$= a \, \mu_0 \left(\frac{\partial u}{\partial y} \right)_0 + u_1 \rho_0 v_0 a. \tag{8}$$

If we divide equation (8) by $\rho_1 u_1^2 a$, combine the second and third terms, and break the first term into two terms, we have

$$\int_0^\delta \frac{\partial}{\partial s} \frac{r}{a} \frac{\rho u}{\rho_1 u_1} \left(1 - \frac{u}{u_1} \right) dy + \frac{1}{\rho_1 u_1^2 a} \left[\int_0^\delta \frac{r}{a} \frac{\rho u}{\rho_1 u_1} \left(1 - \frac{u}{u_1} \right) dy \right] \frac{\partial}{\partial s} \rho_1 u_1^2 a$$

$$+ \frac{1}{u_1} \int_0^\delta \frac{r}{a} \left(1 - \frac{\rho u}{\rho_1 u_1} \right) \frac{\partial u_1}{\partial s} \, dy = \frac{\mu_0 \left(\frac{\partial u}{\partial y} \right)_0}{\rho_1 u_1^2} + \frac{\rho_0 v_0}{\rho_1 u_1} . \tag{9}$$

We now define the displacement and momentum thicknesses in terms of axially symmetric flow to account for the transverse curvature effect of a thick boundary layer.

Mass Flow Defect: $\displaystyle\int_0^{\delta^*} 2 \pi r \, \rho_1 u_1 \, dy = \int_0^\delta 2 \pi r \, (\rho_1 u_1 - \rho u) \, dy.$ (10)

8

Momentum Flow Defect:
$$\int_0^\theta 2\pi r \, \rho_1 u_1^2 \, dy = \int_0^\delta 2\pi r \, \rho(uu_1 - u^2) \, dy.$$

$$\tag{11}$$

If it is now assumed that $\cos \omega \equiv \cos \omega_0 = \cos \omega_{ec}$, equations (10) and (11) can be written

$$\delta_1 = \int_0^\delta \frac{r}{a} \left(1 - \frac{\rho u}{\rho_1 u_1} \right) dy, \tag{12}$$

where

$$\delta_1 \equiv \delta^* - \frac{\delta^{*2} \cos \omega}{2a} \tag{13}$$

and

$$\theta_1 = \int_0^\delta \frac{r}{a} \left(1 - \frac{u}{u_1} \right) \frac{\rho u}{\rho_1 u_1} \, dy \tag{14}$$

where

$$\theta_1 \equiv \theta - \frac{\theta^2 \cos \omega}{2a} . \tag{15}$$

When equations (12) and (14) are substituted into equation (9), and dx cos ω substituted for ds, we obtain the integral momentum equation for axisymmetric flow with suction:

$$\frac{d\theta_1}{dx} + \theta_1 \left[\frac{(\delta_1/\theta_1)}{u_1} \frac{du}{dx} + \frac{1}{a \rho_1 u_1^2} \frac{d}{dx} \, a \rho_1 u_1^2 \right] = \frac{C_f}{2} \sec \omega + \frac{v_0}{u_1} \frac{T_1}{T_0} \sec \omega$$

where

$$C_f = \frac{\mu_0 \left(\frac{\partial u}{\partial y} \right)_0}{1/2 (\rho_1 u_1^2)} \tag{16}$$

and

$$\frac{T_1}{T_O} = \frac{\rho_O}{\rho_1}$$

(from assumption of no pressure change across boundary layer).

In place of the quantity δ_1/θ_1, Durand and Potter recommend the substitution of $(\delta^*/\theta)_{2d}$. This is shown to be a very good approximation, and greatly reduces the complexity of the calculations.

Equation (16) is a linear, first order differential equation, the solution of which can be given as

$$\theta_1 = \frac{\theta_1(o)}{G(x)} + \frac{1}{G(x)} \int_o^x W(x)\ G(x)\ dx \tag{17}$$

where, with $\delta_1/\theta_1 = (\delta^*/\theta)_{2d}$,

$$G(x) = \exp \int_o^x \left[\frac{(\delta^*/\theta)_{2d}}{u_1} \frac{du}{dx} + \frac{1}{a\ \rho_1\ u_1^2} \frac{d}{dx} (\rho_1\ u_1^2\ a) \right] dx \tag{18}$$

and

$$W(x) = \frac{C_f \sec \omega}{2} + \frac{v_O}{u_1} \frac{T_1}{T_O} \sec \omega. \tag{19}$$

If it is assumed that the boundary layer calculations will be started at the throat with $x = 0$, $M_1 = 1$, and $\theta_1(o) = 0$, then equation (17) becomes

$$\theta_1 = \frac{1}{G(x)} \int_o^x W(x)\ G(x)\ dx. \tag{20}$$

To solve equation (20) it is necessary to find methods of evaluating C_f, v_O/u_1, and $(\delta^*/\theta)_{2d}$. These items are discussed below.

10

Skin Friction Coefficient, C_f, and Form Factor, $(\delta^*/\theta)_{2d}$

Lew and Fanucci [4] give an exact solution for uniform suction on a flat plate in compressible flow. They point out that when μ is proportional to T, the equations have the same form in both the incompressible and compressible cases, and all the results for the incompressible case can be used. Appendix B shows the equivalence for the integral equations.

Iglisch [13] has developed an exact solution for two-dimensional incompressible flow with suction. Skin friction coefficient and $(\delta^*/\theta)_{2d_{inc}}$ are given as functions of $\sqrt{\xi_{inc}}$. The nondimensional distance along the plate, ξ_{inc}, is defined as $\xi_{inc} = (v_0/u_1)^2 Re_{inc}$, where $Re_{inc} = \rho_0 u_1 x/\mu_0$. To obtain the corresponding compressible values in terms of the freestream Reynolds number it should be observed that

$$Re_{inc} = (Re_{comp})_{wall} = (T_1/T_0)^2 Re_{comp},$$

since $\mu \sim T$ and the static pressure is assumed constant through the boundary layer. Thus the results of Iglisch for C_f and $(\delta^*/\theta)_{2d_{inc}}$ can be used directly as functions of

$$\frac{T_1}{T_0}\sqrt{\xi} \quad \text{instead of} \quad \sqrt{\xi_{inc}} \ .$$

Figure 4 was taken from Table II in Iglisch. The value of $(\delta^*/\theta)_{2d_{inc}}$ obtained from the figure is used in the following equation (derived in Reference 14) to get $(\delta^*/\theta)_{2d}$:

$$(\delta^*/\theta)_{2d} = (\delta^*/\theta)_{2d_{inc}} \frac{T_0}{T_1} + \frac{T_{aw}}{T_1} - 1. \tag{21}$$

If pressure gradient is to be taken into account, the results of Cohen and Reshotko [15] can be used. They give the following equation for δ^*/θ:

$$\delta^*/\theta = H_{t_r} + \frac{\gamma - 1}{2} M_1^2 (H_{t_r} + 1), \tag{22}$$

where H_{t_r} is a function of wall to freestream enthalpy ratio and a pressure gradient parameter, n. Determination of the pressure gradient parameter is discussed in Reference 15.

The following equation for C_f, which includes the effect of pressure gradient, is given in Reference 15:

$$\frac{C_f}{2} \sqrt{\overline{Re_1}} \ (T_1/T_O)^2 = \ell \sqrt{\frac{-\frac{x}{u_1}\frac{du_1}{dx}}{n \ T_1/T_O}} \ . \tag{23}$$

(ℓ is a function of n and T_O/T_{T_1}

The influence of pressure gradient was not accounted for in the present study.

Suction Velocity Ratio, v_O/u_1

Since the velocity ratio is the dominant factor in reducing the boundary layer height by suction, it is necessary to relate this ratio to the pore or hole geometry used on the nozzle wall. In the theoretical analysis, it is assumed that a uniform normal velocity exists at the wall. In any physical case, it will be necessary to use an array of holes with discrete spacing. By making the hole size and spacing small enough, it should be possible to obtain a nearly uniform normal velocity.

If the gradients in the boundary layer have a negligible effect on the flow through the holes, the holes may be considered as tubes with reservoir conditions equal to the local wall static pressure and local wall temperature. If the tube exit pressures are assumed to be negligible, the problem becomes one of determining the "choking" mass flow through tubes of varying L/D and Reynolds number. In the design of a nozzle, the length "L" will be the wall thickness which will be determined from a compromise involving considerations of thermal conductivity, structural length, and the suction mass flow. It is desirable to have the walls thick to assure adequate strength and to minimize the number of cooling coils that must be used on the walls; however, at low Reynolds number it is necessary to minimize the wall thickness to allow high suction mass flows with the attendant high suction velocity ratios.

There is one regime where simple, accurate estimates can be made of the mass flow through tubes. This is the free molecular flow regime, where it is assumed that the gas density is so low that the molecules collide with the walls many times before they collide with one another. In this limiting regime, the effects of L/D can be readily assessed using published graphs (Reference 16, for example).

12

For the particular case of a sharp-edged orifice, the continuum mass flow has been computed theoretically and roughly checked experimentally, as shown in Reference 17. Here it is shown that with adequate pressure ratio (greater than 13) the ratio of actual mass flow to that existing with a uniformly choked opening is about 85%. Further, this reference presents the experimentally determined change in mass flow ratio as the Reynolds number is reduced to free molecular conditions. This data was limited to $L/D = 1/40$. Brown, et al. [18] give experimental results at higher values of L/D. Data from both References 17 and 18 are shown in Figure 5, along with free molecular values of various L/D. The Reynolds number, Re_D, is based on sonic flow.

While the data in Figure 5 all have similar levels at small values of the parameter $64/Re_D\, L/D$, at the higher values of this parameter the data show a definite trend with L/D. Thus at the higher values of $64/Re_D\, L/D$, tubes with larger L/D ratios have lower mass flow ratios. The final value attained is the free molecular flow value, and the curve then ceases to change with $64/Re_D\, L/D$.

Using Figure 5 with suitable fairing, $\dot{m}/\dot{m}_*$ is known and v_o is given by the equation (negative sign for suction)

$$v_o = - \frac{\dot{m}_{s_*}\left(\dfrac{\dot{m}_s}{\dot{m}_{s_*}}\right)}{\rho_o\, \Delta A_o}$$

where

$\dot{m}_s$ is the suction mass flow rate,

$\dot{m}_{s_*}$ is the suction mass flow rate with uniform sonic flow through the holes,

ρ_o is average density at the wall, and

ΔA_o is wall area

for the nozzle Δx considered. Using standard equations for sonic mass flow (Reference 19, p. 82), the ratio v_o/u_1 can be expressed as

$$v_o/u_1 = - .0165 \sqrt{\frac{R}{\gamma}}\, \frac{\phi}{M_1}\, \frac{\dot{m}_s}{\dot{m}_{s_*}}\, \sqrt{T_o/T_1} \qquad (24)$$

where ϕ is the ratio of open area to total wall area.

B. Determination of the Boundary Layer Thickness

All of the discussion up to this point has concerned computation of the displacement thickness, Mach number, and nozzle radius. Of equal importance is the determination of the actual thickness of the boundary layer, δ. It is this quantity which determines the size of the uniform test core. In this development, δ is defined as the height where the velocity has reached either 99% or 99.9% of the free-stream velocity. The equations are set up so that either of these or any other desired velocity ratio can be specified.

Equating Equations (12) and (13) gives

$$\delta^* - \frac{\delta^{*2} \cos \omega}{2a} = \int_{o}^{\delta} \frac{r}{a}\left(1 - \frac{\rho u}{\rho_1 u_1}\right) dy. \tag{25}$$

Substituting $r = a - y \cos \omega$, and using y_e for δ, where the subscript e is used to denote the edge of the boundary layer, we have

$$\delta^* - \frac{\delta^{*2} \cos \omega}{2a} = \int_{o}^{y_e}\left(1 - \frac{\rho u}{\rho_1 u_1}\right) dy - \frac{\cos \omega}{a}\int_{o}^{y_e}\left(1 - \frac{\rho u}{\rho_1 u_1}\right) y \, dy. \tag{26}$$

For ease of computation, equation (26) has been further simplified by breaking up the integrals as follows:

$$\delta^* - \frac{\delta^{*2} \cos \omega}{2a} = y_e - \int_{o}^{y_e} \frac{\rho u}{\rho_1 u_1} dy - \frac{\cos \omega}{a}\left[\frac{y_e^2}{2} - \int_{o}^{y_e} \frac{\rho u}{\rho_1 u_1} y \, dy\right]. \tag{27}$$

Evaluation of the integrals in equation (27) will now be discussed. The development draws heavily on the work of Lew and Romano [6], which has been summarized in Appendix A. The first integral may be written

$$X \equiv \int_{o}^{y_e} \frac{\rho u}{\rho_1 u_1} dy = \int_{o}^{\tau_e} \frac{\rho u}{\rho_1 u_1} \frac{dy}{dt} \delta_t \, d\tau, \tag{28}$$

where the variable of integration has been changed from y to τ (see Appendix A). It is shown in Appendix A that

$$\frac{dy}{dt} = L \frac{\rho_1}{\rho} \frac{T_1}{T_0} .$$

With this substitution, we have

$$X = L \, \delta_t \frac{T_1}{T_0} \int_0^{\tau_e} \frac{u}{u_1} \, d\tau. \tag{29}$$

Substituting for δ_t the expression $\delta_t = 2\lambda/\text{Re} \, \bar{v}_0$ (see Appendix A) and using the definitions of Re and $\bar{v}_0$ given in Appendix A, equation (29) simplifies to

$$X = \frac{2\lambda \, \mu_0}{v_0 \, \rho_0} \frac{T_1}{T_0} \int_0^{\tau_e} \frac{u}{u_1} \, d\tau = \frac{2\lambda \, \mu_0}{v_0 \, \rho_1} \int_0^{\tau_e} \frac{u}{u_1} \, d\tau. \tag{30}$$

To carry out the indicated integration, it is necessary to assume a velocity profile. In Reference 9, a velocity profile of the form $u/u_1 = \sin \frac{\pi y/\delta}{2}$ is used and good correlation with experimentally obtained values of δ is shown. An exact solution for the suction case is given in Reference 4, but the computations are laborious. Lew and Romano suggest an exponential profile of the form $u/u_1 = 1 - e^{-\tau}(1 - \tau K)$ (see Appendix A). This profile showed good agreement with an exact solution for the two-dimensional asymptotic suction case [4] at Mach number 10 and $T_0/T_1 = 4$. For the same conditions, it over-estimated the boundary layer thickness for the no-suction case (exact solution, Reference 20) by about 20%. Substituting the above velocity profile (equation (11) of Appendix A) and integrating, we get

$$X = \frac{2\lambda \, \mu_0}{v_0 \, \rho_1} [\tau_e - 1 + K], \tag{31}$$

where terms involving $e^{-\tau_e}$ and $e^{-2\tau_e}$ have been dropped since they are negligible. λ is determined by Lew and Romano's solution, equation (13), Appendix A.

15

$$\xi = \frac{1}{2} (T_0/T_1)^2 \left[\frac{\lambda(3\lambda + 5)}{\lambda + 1} + 5 \ln \frac{(\lambda + 1)}{(2\lambda + 1)} \right] , \tag{32}$$

where

$$\xi = (v_0/u_1)^2 \frac{\rho_1 u_1 x}{\mu_1} .$$

All quantities needed to evaluate ξ are known, and λ is determined by an iteration of equation (32). With λ known, K may be evaluated, and τ_e determined by equation (11) of Appendix A for $u/u_1 = .999$, or whatever velocity ratio has been selected to define the edge of the boundary layer.

The second integral in equation (27) may be written (following a development similar to that for the first integral):

$$Y \equiv \int_0^\delta \frac{\rho u}{\rho_1 u_1} y \, dy = \frac{2\lambda \mu_0}{v_0 \rho_1} \int_0^{\tau_e} \frac{u}{u_1} y \, d\tau. \tag{33}$$

The expression for y as a function of τ is obtained by integrating equation (6) of Appendix A, which may be written in the form

$$y(\tau) = \frac{2\lambda \mu_0}{v_0 \rho_1} \frac{T_0}{T_1} \int_0^\tau \left[1 + \frac{u}{u_1} \left(\frac{T_1}{T_0} - 1 + \frac{u_1^2}{2c_p T_0} \right) - \frac{u^2}{2c_p T_0} \right] d\tau. \tag{34}$$

Substituting the exponential velocity profile for $\dot{u}/u_1$ and carrying out the integration, one obtains

$$y^{(\tau)} = \frac{2\lambda \mu_0}{v_0 \rho_1} \frac{T_0}{T_1} Q, \tag{35}$$

16

where

$$Q = \tau - \frac{\gamma - 1}{2} M_1{}^2 \frac{T_1}{T_O} \left[\tau + 2e^{-\tau} - 2Ke^{-\tau} (\tau + 1) - \frac{1}{2} e^{-2\tau} (1 - 2\tau K - K) \right.$$

$$\left. - K^2 e^{2\tau} \left(\frac{\tau^2}{2} + \frac{2\tau + 1}{4} \right) - \frac{3}{2} + \frac{3}{2} K + \frac{K^2}{4} \right] \tag{36}$$

$$+ \left(\frac{T_1}{T_O} - 1 + \frac{\gamma - 1}{2} M_1{}^2 \frac{T_1}{T_O} \right) \left[\tau + e^{-\tau} - e^{-\tau} (\tau + 1) K - 1 + K \right] .$$

If we now replace the integral expressions in equation (27) by equations (31) and (33), and use equation (35) for y, we get

$$\delta^* \left(1 - \frac{\delta^* \cos \omega}{2a} \right) = y_e - \frac{2\lambda \mu_O}{v_O \rho_1} [\tau_e - 1 + K]$$

$$- \frac{\cos \omega}{a} \left[\frac{y_e^2}{2} - \left(\frac{2\lambda \mu_O}{v_O \rho_1} \right)^2 \frac{T_O}{T_1} \int_0^{\tau_e} \frac{u}{u_1} Q d\tau \right] . \tag{37}$$

In this equation δ^*, a, μ_O, v_O, ρ_1, T_O/T_1, and $\cos \omega$ are all known quantities. The term y_e is given by equation (35) which becomes, after terms involving $e^{-\tau_e}$ are dropped (τ_e is always of the order of 4.5 to 8),

$$y_e = \frac{2\lambda \mu_O}{v_O \rho_1} \frac{T_O}{T_1} \left[\tau_e - \left(\frac{\gamma - 1}{2} M_1{}^2 \frac{T_1}{T_O} \right) \left(\tau_e - \frac{3}{2} + \frac{3}{2} K + \frac{K^2}{4} \right) \right.$$

$$\left. + \left(\frac{T_1}{T_O} - 1 + \frac{\gamma - 1}{2} M_1{}^2 \frac{T_1}{T_O} \right) (\tau_e - 1 + K) \right] . \tag{38}$$

In the above set of equations, λ and all things determined by it (namely, K, τ_e, $(u/u_1)_e$ and Q) must be considered as a function of a flat plate x, which we could call x'. They cannot be evaluated at the particular nozzle x under consideration, since then equation (37) would be overspecified. It is noted that λ is determined by equation (32) and

17

the x' dependence enters as the Reynolds number. Thus, to determine δ, we assume for the moment that the boundary layer is on a flat plate with a known Mach number, T_O/T_1 and δ^*, and vary the x' until equations (37) and (38) are simultaneously satisfied. The term δ is, of course, the value of y_e for which the equations are satisfied.

One problem occurred in the computation of δ by the method outlined herein. For sufficiently high unit Reynolds numbers in the suction case, no solution for δ could be obtained, since for the δ^*, Mach number and other conditions given (which are those occurring in a nozzle, not a flat plate), the boundary layer height on a flat plate does not reach a high enough value at any x' to satisfy the equations. Suction boundary layers do not continue to grow indefinitely, but reach a maximum height at the point where the suction velocity balances the rate of growth. This limitation was encountered only once in the course of this study. The conditions for which no solution could be reached occurred in a 10° half-angle nozzle at a Mach number of 7.66, a unit Reynolds number of 5200/inch, with a suction velocity ratio v_O/u_1 of -.0305 (the minus sign indicates suction). The wall-to-freestream temperature ratio, T_O/T_1, was 1.88. The limitation thus apparently occurs only at relatively high unit Reynolds numbers and suction velocity ratios (the open area in the above case was 60% of the wall area) even for highly cooled walls. For most cryopumped wind tunnels, it is considered that the limiting conditions would rarely be encountered.

IV. METHODS OF CALCULATION

A. Displacement Thickness, δ^*

We now proceed to discuss the methods of solving equation (20). Two basic approaches are possible, depending on what information is given. In both methods, it is necessary to integrate equation (20) numerically. Also, an iterative procedure is necessary in both methods.

The first method attacks the problem of calculating the Mach number and uniform core radius with a given nozzle shape and porosity distribution. The procedure is of the iterative type because the Mach number depends on the magnitude of the suction, and in turn the suction mass flow depends on the Mach number distribution. It is necessary to assume hole diameter D as a function of x. It is considered that the hole diameters can be safely made to be 20% of the expected boundary layer thickness. The calculations are not sensitive to the hole size chosen, and thus conservative values should be used. The nozzle is divided into several increments of length, Δx. The calculation is not particularly sensitive to the number of increments chosen. For Mach numbers of the order of 12, twenty increments usually gives an accuracy consistent with the accuracy of the theory. The calculation is begun

at the first x and proceeds down the nozzle, $\delta*$ and Mach number being calculated at each x. It is necessary to compute δ only at the last x. To begin the calculation, it is necessary to assume a value of the Mach number at the first station considered. In the initial portion of the nozzle, where the boundary layer is thin, a good first guess is the Mach number which would occur with no boundary layer and no suction. Further down the nozzle, it is better to add small Mach number increments to the Mach number at the previous station until agreement is obtained.

The calculation is summarized as follows: For x_n, assume a Mach number M_1, where n refers to the nozzle location. Compute p_1, T_1, ρ_1, u_1, from known stagnation conditions and isentropic equations.

$$\mu_1 = \mu_{ref} \frac{T_1}{T_{ref}} \quad \text{or} \quad \mu_1 = \left(\frac{T_1}{T_{ref}}\right)^{3/2} \left(\frac{T_{ref} + S}{T_1 + S}\right) \mu_{ref}$$

$$\left[\begin{array}{l} \underline{\text{Note}}: \text{ If throughout most of the nozzle} \\ \text{the static temperature is below } 180°R, \\ \text{the linear law will give the better result} \\ \text{for nitrogen.} \end{array}\right]$$

$$Re_1 = \frac{\rho_1 u_1 x}{\mu_1}$$

$$Re_D = \sqrt{\frac{\gamma}{R}} \frac{\rho_1}{\sqrt{T_1}} \frac{D}{\mu_*} \frac{1}{\left(1 + \frac{\gamma - 1}{2}\right)^{\frac{\gamma+1}{2(\gamma-1)}}} = \text{Reynolds number based on hole diameter and sonic conditions.}$$

where μ_* is given by $\mu_* = \mu_{ref} \frac{T_0}{T_{ref}} \left(\frac{1}{1 + \frac{\gamma - 1}{2}}\right)$

$$P_{1_{avg.}} = \frac{P_{1_{x_n}} - P_{1_{x_{n-1}}}}{2} = \text{average pressure over the interval } \triangle x.$$

ϕ'/ϕ = same as $\dot{m}/\dot{m}_*$ and is read from Figure 5 at proper value of $64/Re_D \; L/D$.

$$v_O/u_1 = -.0165 \sqrt{R/\gamma} \; \frac{\phi}{M_1} \frac{\phi'}{\phi} \sqrt{T_O/T_1}$$

$$T_{aw} = T_1 \left(1 + \frac{\gamma - 1}{2} M_1^2 \sqrt{Pr} \right) = \text{adiabatic wall temperature.}$$

$$\xi = (v_O/u_1)^2 \; Re_1$$

$\dfrac{C_f}{2} \sqrt{Re_1}$ is taken from Figure 4 at proper value of $\sqrt{\xi} \; \dfrac{T_1}{T_O}$

$(\delta^*/\theta)2d_{inc}$ is taken from Figure 4 at proper value of $\sqrt{\xi} \; \dfrac{T_1}{T_O}$

$$(\delta^*/\theta)2d = (\delta^*/\theta)2d_{inc} \; (T_O/T_1) + \frac{T_{aw}}{T_1} - 1$$

$$\left[\frac{(\delta^*/\theta)_{2d}}{u_1} \right]_{avg} = \frac{\left[\dfrac{(\delta^*/\theta)_{2d}}{u_1} \right]_{x_n} + \left[\dfrac{(\delta^*/\theta)_{2d}}{u_1} \right]_{x_{n-1}}}{2}$$

$$\Delta u_1 = (u_1)_{x_n} - (u_1)_{x_{n-1}}$$

$$G(x) = \frac{(a \, \rho_1 \, u_1^2)_{x_n}}{(a \, \rho_1 \, u_1^2)_{x=0}} \qquad \exp \sum_{x_1}^{x_n} \Delta u_1 \left[\frac{(\delta^*/\theta)_{2d}}{u_1} \right]_{avg.}$$

$$W(x) = \frac{C_f}{2 \cos \omega} + \frac{v_O}{u_1} \frac{T_1}{T_O} \frac{1}{\cos \omega}$$

$$[G(x) \; W(x)]_{avg.} = \frac{[G(x) \; W(x)]_{x_n} + [G(x) \; W(x)]_{x_{n-1}}}{2}$$

Note: When $x_{n-1} = 0$, take $G(x) \; W(x) = 3 \; (C_f/2 \cos \omega)$,
since $C_f = \dfrac{C_{f_{avg}}}{2}$ and $G(x)$ is of the order of 1.

$$\theta_1 = \frac{1}{G(x)} \sum_{x_1}^{x_n} [G(x)\ W(x)]_{avg.}\ \Delta x$$

$$\delta_1 = \theta_1\ (\delta*/\theta)_{2d}$$

$$\delta* = \frac{a}{\cos \omega} \left[1 - \sqrt{1 - \frac{2 \cos \omega}{a} \delta_1} \right]$$

$$r_{ec} = a - \delta* \cos \omega$$

$$\dot{m}_s/\dot{m}_* = \sqrt{T_{T_1}/T_0}\ \ \frac{\displaystyle\sum_{o}^{x_n} P_{1_{avg.}}\ \Delta A_0\ \phi'}{P_{T_0}\ A_*}$$
(Summation of suction flow up to x_n divided by the total nozzle flow)

$$A/A_* = (r_{ec}/r_*)^2 \left(\frac{1}{1 - \dfrac{\dot{m}_s}{\dot{m}_*}} \right).\qquad **$$

** This equation results from forming the ratio of the flow per unit area at any nozzle station to the flow per unit area at the throat.

$$\frac{\dfrac{\dot{m}_{ec}}{A_{ec}}}{\dfrac{\dot{m}_*}{A_*}} = \frac{\sqrt{\dfrac{\gamma}{R}}\ \dfrac{P_{T_1}}{T_{T_1}}\ \dfrac{M}{\left(1 + \dfrac{\gamma - 1}{2} M^2\right) \gamma + \dfrac{1}{2(\gamma - 1)}}}{\sqrt{\dfrac{\gamma}{R}} \dfrac{P_{T_1}}{T_{T_1}}\ \sqrt{(2/\gamma + 1)^{\gamma + 1/\gamma - 1}}} = \frac{A_*}{A}$$

where $\dot{m}_{ec}$ is the mass flow in the expansion core at the station considered. Thus,

$$\frac{A}{A_*} = \frac{A_{ec}}{A_*}\ \frac{\dot{m}_*}{\dot{m}_{ec}} = \frac{A_{ec}}{A_*}\ \frac{\dot{m}_*}{\dot{m}_* - \dot{m}_s} = \frac{A_{ec}}{A_*} \left(\frac{1}{1 - \dfrac{\dot{m}_s}{\dot{m}_*}} \right).$$

If M_1 assumed is within a specified tolerance of the Mach number given by A/A_*, the calculation of δ^* and Mach number is complete. Otherwise, a new value of M_1 is assumed and the calculation repeated.

The second method begins with a known Mach number distribution and computes the required wall radius and uniform core size. It is necessary to specify either the porosity distribution (open area to total wall area, even though the wall area is not known) or the suction mass flow distribution, $\dot{m}_s/\dot{m}_*$. Since the Mach number is known, all Mach number dependent items can immediately be computed. If it is the porosity distribution (percent open area) which has been specified, the calculation proceeds in exactly the same manner as the first method up to the $G(x)$ calculation. A value for the wall radius is now assumed. Then θ_1, δ_1, and $\dot{m}_s/\dot{m}_*$ are evaluated as before; r_{ec} is obtained from the equation

$$\frac{A}{A_*} = (r_{ec}/r_*)^2 \left(\frac{1}{1 - \frac{\dot{m}_s}{\dot{m}_*}} \right) .$$

The value of δ^* is given by

$$\delta^* = \delta_1 - \frac{r_{ec}}{\cos \omega} + \sqrt{\left(\frac{r_{ec}}{\cos \omega} - \delta_1 \right)^2 + 2 \frac{r_{ec}}{\cos \omega} \delta_1} .$$

The wall radius a may now be computed from $a = r_{ec} + \delta^* \cos \omega$. This new value is now used throughout the computation and the process repeated until the computed a agrees with the assumed a to within a prescribed tolerance. In all computations performed during this study, this procedure always converged.

If it is the suction weight flow ratios which are specified, a wall radius is assumed and v_0/u_1 computed from the equation

$$v_0/u_1 = - \frac{R \, \Delta\dot{m}_s \, T_0}{u_1 \, \Delta A_0 \, P_1} ,$$

where $\Delta\dot{m}_s$ and ΔA_0 are the incremental suction mass flow and wall area for the Δx considered. θ_1 and δ_1 are computed as in the first method; r_{ec}, δ^*, and a new a are computed as above, and the same iterative procedure followed. After a is found, the required ϕ is given by

$$\phi = \frac{\phi'}{\phi'/\phi} = \frac{\Delta\dot{m}_s \sqrt{T_O}}{\frac{\phi'}{\phi} P_1 \sqrt{\frac{\gamma}{R}}} \left(1 + \frac{\gamma - 1}{2}\right)^{\frac{\gamma+1}{2(\gamma-1)}}$$

where ϕ'/ϕ is the same as $\dot{m}/\dot{m}_*$ and is known from Figure 5.

B. **Boundary Layer Thickness, δ**

    With δ^* and Mach number known from either of the above two methods the thickness of the boundary layer is computed by simultaneously satisfying equations (37) and (38). In these equations δ^*, a, μ_O, v_O, ρ_1, T_1/T_O, and cos ω are all known. The computation proceeds as follows:

(1) Assume an x'.

(2) Find λ by an iteration of equation (32). A table of values of this function is presented in Table II. The assumed value of x' is used for x in equation (32).

(3) $K = -\ 1/2 \left(\dfrac{1 + 2\lambda}{1 + \lambda}\right)$

(4) τ_e is determined from $(u/u_1)_e = 1 - e^{-\tau_e} (1 - \tau_e K)$. The value of $(u/u_1)_e$ is that which defines the boundary layer thickness (usually taken as .999, but in this procedure it is arbitrary).

(5) A value for y_e can now be computed from equation (38) and substituted into equation (37). The integral in the last term of equation (37) can be evaluated either numerically, graphically or analytically. u/u_1 is given by $1 - e^{-\tau} (1 - \tau K)$ and Q by equation (36). Because of the large number of terms in this expression, a graphical or numerical integration procedure is recommended.

(6) If equation (37) is not satisfied with the assumed x', a larger value is assumed and the process repeated; δ is the value of y_e for which equation (37) is satisfied.

In the case of no suction, $(v_O = 0)$, the term

$$\frac{2\lambda\ \mu_O}{v_O\ \rho_1}$$

is indeterminate since $\lambda = 0$ when $v_O = 0$. An expansion of equation (32) for the case when $\lambda \to 0$ shows that

$$\frac{2\lambda\ \mu_O}{v_O\ \rho_1}$$

can be replaced by

$$\frac{1.2\ x'}{\sqrt{\dfrac{\rho_1\ u_1}{\mu_1}}}\ .$$

V. EXPERIMENTAL INVESTIGATION AND COMPARISON WITH THEORY

A. Experimental Arrangement

An experimental program was devised to provide a check on the theoretical calculations.* A sketch of the experimental layout is presented in Figure 6. During operation, the nitrogen used as the test gas is obtained by vaporizing liquid nitrogen. This gas passes through the 1.5-K.W. heater to the stilling chamber and then into the nozzle. Part of the flow passes through the nozzle pores to cryopump coils surrounding the nozzle, while the rest continues through the nozzle into the vane-type "diffuser" that serves as a precooler. This gas passes between the vanes to the remaining cryopump coils. The cryopump is cooled by gaseous helium from a 350-watt refrigerator. A liquid-nitrogen cooled shield reduces the ratiation load to the cryopump. A roughing pump is used for initial tank evacuation, and a diffusion pump is used to remove any noncondensible gases.

The nozzle schematic is presented in Figure 7. The nozzle is a 13° half-angle cone fabricated in two sections. The forward section

---

* Experiments were conducted in the Hyperaltitude Facility of the Environmental Division of the U. S. Naval Missile Center, Point Mugu, California.

was machined from solid copper and includes the contraction section, the throat, and the supersonic section to a diameter of 2". The 9/32" diameter throat is a cylinder about one diameter long with the corners slightly rounded.

The second section is the porous section that extends from the 2" diameter to the 12" diameter. It was rolled from a 3/16" sheet of copper after the pores had been drilled. The hole pattern and the resulting porosity are also given in Figure 7. The porosity distribution is essentially linear with axial distance. The hole radii were selected to keep the ratio of the hole radius to local boundary layer height equal to about .1; however, near the front of the porous section this ratio approached .6.

The liquid-nitrogen cooling coils were soldered on this section with approximately 6" between coils. The coils did not cover any of the pores.

After joining, the two sections were given the final machining so the nozzle coordinates are within 1% of a true 13° half-angle cone.

B. Instrumentation

Test section pitot pressure was measured on an Alphatron (NRC Model 520). A calibration made prior to the test showed that in the range of most of the testing (100μ - 300μ), the instrument was as accurate as the scale could be read. This corresponds to from ± 5% to ± 1.7%. Limited data taken below 100μ required corrections of less than 10% to achieve reading accuracy.

Stagnation pressure was measured using a Bourdon gage at pressures above 20 mm Hg and a McLeod gage for lower pressures. The accuracy of this system was approximately ± 2%.

Tunnel static pressure was measured using a thermocouple gage designed for the low-micron range. No calibration was available, but the reading accuracy and the repeatability were approximately ± $.2\mu$ in the testing range.

C. Experimental Results

1. Porous Wall Nozzle

Radial pitot probe surveys were made for a range of stagnation temperatures and pressures. In general a .312" O.D., .270" I.D. pitot tube was used. Since these dimensions are the same order of magnitude as the mean free path of freestream gas, tests were made on a larger

25

probe (.875" O.D., .785" I.D.) and a smaller probe (.125" O.D., .106" I.D.) to determine the effect of probe size on the indicated pitot pressure. The results of these tests, shown in Figure 8, were used to correct the pitot probe surveys. Only the data taken with stagnation pressures less than .5 psia required corrections of 10% or more.

These corrected surveys are presented in Figure 9. For these stagnation conditions, the nozzle developed Mach numbers ranging from 9.15 to 11.0 at freestream Reynolds numbers ranging from 100/inch to 500/inch. At the lowest Reynolds number, the pitot pressure ratio is lower than would be expected. Despite the region of uniform pitot pressure (obtained with the .125" O.D. probe), it appears that the boundary layer has merged and the stream stagnation pressure is decreasing. Since the pitot pressure is ratioed to the upstream stagnation pressure, this would account for the low ratio. As will be shown in the next section, this is consistent with the theoretical calculations.

At the higher Reynolds number the profiles show an increasing pitot pressure as the probe moves from the center. This is typical of low-density conical nozzles when they are operated at higher densities. The extent of this higher density regime can be estimated from the ratio of boundary layer height to test section radius (δ/a). This is illustrated in Figure 10, where the ratio of the pitot pressure at the edge of the core to the centerline pitot pressure has been plotted versus the ratio (δ/a) for a series of conical nozzles. The data covers the Mach number range 4.5 - 11.0 and cone half-angles from 10° to 20°. From this plot it can be seen that as (δ/a) is reduced below about .7, the pitot profile variations exceed 5%. Thus, to avoid transverse Mach number gradients, simple, conical nozzles must be operated at low densities in order that (δ/a) exceeds .7. For higher density operation, it appears necessary to use a smaller cone angle or to contour the nozzle walls.

2. Solid Wall Nozzle

In order to obtain a direct comparison of a solid-wall nozzle and a porous-wall nozzle, the exterior of the nozzle was covered with aluminum foil. While this prevented any outflow, it did leave the interior nozzle wall rough due to the closed pores; however, it was felt that these closed pores would not present any greater disturbances than they had when used as a porous wall.

The pitot profiles obtained from this solid-wall nozzle are presented in Figure 11. The corresponding porous-wall data are also presented. From a comparison of the two sets of data, it is clear that the main effect of the porous wall was to increase the Mach number while maintaining approximately the same boundary layer height.

26

D. Comparison of Theory and Experiment

Theoretical calculations were made for the various test conditions, and the comparison between the theoretical and experimental Mach numbers and boundary layer heights is presented in Figures 12 and 13. For direct comparison the theoretical values of Reynolds number/inch have been used as the abscissa for both sets of data.

Figures 12 and 13 show that, with the exception of the lowest Reynolds number/inch point, the theory predicts the Mach number to within 5% and the boundary layer height to within 10%. Since these calculations were made using a 145°R nozzle wall, while in the experiment the throat block was at a higher temperature (about 285°R), calculations were also made to assess the effect of this temperature distribution. The results showed that the temperature distribution changed the Mach number by less than .5% and the boundary layer height by less than 2%. The boundary layer calculation on the lowest Reynolds number/inch point showed that the boundary layers had merged. This agrees with the experimental results discussed in the previous section.

Although the ratio of mean free path to pore radius varied from about .1 to 1.3, the suction mass flow was computed using free molecular flow values of $\dot{m}/\dot{m}_*$ for all conditions. It is estimated that this simplification reduces the total suction mass flow by less than 10%. Since this calculated suction mass flow varied from 7% to 17% of the throat mass flow, the error is less than 2% of the throat mass flow.

The experimental data with comparable stagnation conditions were also used to determine the suction mass flow by assuming that the difference between the exit Mach numbers for the solid wall and the porous wall was due to the suction mass flow reducing the exit mass flow. In this case the suction mass flow is determined from

$$\frac{\dot{m}_{out}}{\dot{m}_*} = 1 - \frac{(A/A_*) \text{ solid wall}}{(A/A_*) \text{ porous wall}} .$$

The area ratios are determined from the exit Mach numbers. This procedure assumes that the effects of small changes of Reynolds number, velocity profile, and δ/a are negligible. A comparison of the results of these calculations with the theoretical values, presented in Figure 14, appears to justify the above assumptions.

In an attempt to learn more of the details of the flow coming from the pores, temperature and pitot pressures were measured at the exit of a 5/8" diameter pore. Due to the probable nonequilibrium condition of this exiting flow, and the unknown pitot probe errors, the results were only qualitative. The measured temperature was about 250°R and the pressure was about three times tunnel static pressure. Since the temperature and stagnation pressure in the boundary layer reach these values at distances of the order of one mean free path into the boundary layer, these values seem reasonable. The measured exit temperature being above the nozzle wall temperature suggests that nozzle pores with small values of L/D cannot be used to precool the suction flow to wall temperature. For complete cooling, the pore length and diameter both must be sized relative to the tunnel wall mean free path if the tunnel boundary layer temperature rises significantly in distances of the order of the mean free path.

To check the validity of the theory at higher Reynolds numbers, calculations were made on the cooled porous nozzle reported in Reference 8. This 10° half-angle nozzle had a .104" diameter throat, a 1.9" diameter exit, and a maximum porosity of 60%. The comparison of the results of the calculations and the experiments is presented in Figure 15. The theoretical values of Reynolds number/inch have been used as the abscissa. With the exceptions of the two highest Reynolds numbers where the nozzle flow had strong transverse gradients, the theory predicts the Mach number to within 3%. Similarly, with the exception of a few points, the boundary layer heights are in good agreement. The scatter in the boundary layer plots is believed to be due to the difficulty in defining the edge of the boundary layer on the experimental pitot profiles.

VI. COOLING AND SUCTION EFFECTS ON NOZZLE AND TEST CORE SIZE FOR GIVEN MACH NUMBER DISTRIBUTIONS

Machine calculations were carried out using the second theoretical method outlined in Section IV to determine the benefits of wall suction and cooling for a fixed Mach number. A Mach number distribution was assumed and the resulting boundary layer thickness, nozzle diameter, and uniform core thickness were calculated.

A simple, rapid method of arriving at suitable Mach number distributions to use in the calculations was supplied by the first theoretical method, where a given nozzle shape is specified and a nozzle Mach number distribution is predicted. With a few trials using conical wall shapes, it was possible to predict Mach number distributions with exit Mach numbers close to 3, 6, 9, and 12, the range which was of interest in this study. Thus, although the distributions used were not aimed at a particular test section flow field, they do reflect smooth expansions which would closely approximate the flow in actual nozzles of the same test section Mach number, and are adequate for showing trends.

28

It was endeavored at all Mach numbers to pick a throat size such that the resulting uniform core was about six inches in radius. A nozzle length of four feet was used in all calculations, and in most cases resulted in reasonable nozzle wall angles.

Figure 16 shows the nozzle wall radii, boundary layer thicknesses, and uniform core radii which were calculated for four Mach numbers. The Mach number distributions and throat sizes that were used are given in Table I. Nitrogen was assumed as the nozzle fluid. In all cases a wall temperature of 180°R was used, corresponding roughly to that for a wall cooled by liquid nitrogen. Results are given for the no-suction case and for the case where 22% of the nozzle flow is removed via wall suction. A unit Reynolds number range up to about 300 per inch was selected, since for the nozzle size chosen this corresponds approximately to the maximum weight flow which can be accepted by a one-kilowatt cryopump.

It is readily apparent from the figure that large reductions in the boundary layer thickness occur with 22% suction flow. For the Mach number 12 nozzle, δ is reduced about four inches at a unit Reynolds number of 160/inch, corresponding to a flow rate of 2 grams/sec. The uniform core radii, however, are remarkabley close at all Reynolds numbers, so that the net effect of suction in all cases shown in Figure 16 is to reduce the nozzle diameter.

What may be of more importance, however, is the beneficial effect of precooling in the suction case. It is difficult to exactly assess the benefits of the precooling on the nozzle size and core radii, since this is considerably influenced by the nature of the overall enthalpy removal system, in particular, whether a diffuser and precooler are used downstream of the nozzle and how effective they are. In this regard it is probable that the reduced boundary layer in the suction case would aid attempts to diffuse and precool the nozzle flow. A calculation has been made using simple assumptions about the system to provide an estimate of the possible increase in core size due to the use of suction and precooling. If it is assumed in the no-suction case that all of the enthalpy of the incoming flow is removed by the cryopump, and, for the suction case, 22% of the flow goes through the walls where this suction flow is all precooled to 180°R (liquid-nitrogen coolant), then for a stagnation temperature of 1460°R (Mach 12) we have

$$\frac{\dot{w}_{*_{suction}}}{\dot{w}_{*_{no\ suction}}} = \frac{h_{1460°R}}{.78(h_{1460°R}) + .22(h_{180°R})}$$

$$= \frac{235\ cal/gram}{.78(235\ cal/gram) + .22(90\ cal/gram)} = 1.16.$$

Thus the test section area could be increased by 16% with a resulting 7.5% increase in the uniform core size. Somewhat higher suction rates would raise this number, but it is doubtful that suction flows exceeding 30% of the throat flow are practical, especially if it is intended to cool the suction flow to the temperature of the wall.

Figure 17 gives the results of calculations on the effect of various degrees of wall cooling on a, δ and r_{uc} for Mach number 12 and a unit Reynolds number of 800/inch. This corresponds to a flow of ten grams per second for the nozzle size shown. The high Reynolds number was used in this plot to keep the wall mean free path to reasonable values in the adiabatic wall case. Even for this Reynolds number, however, the adiabatic wall mean free path is about 25% of the boundary layer thickness. Results are given for the no-suction case and for a suction case with $\emptyset_{max}$ = .66. Again, large decreases in δ are possible with the use of cold walls, but the uniform core radii are very close in the suction and no-suction cases for any wall temperature. A perhaps surprising feature of the plot is the increase in uniform core radii as the adiabatic wall temperature (no cooling) is approached. Of course, without cooling the nozzle radii get very large, and for the particular case shown here, this would result in a very large wall divergence even if suction were used. Moreover, it is uncertain how successfully such a thick boundary layer could be cooled after leaving the nozzle, and therefore a hot wall may still be inferior to a cold wall with the resulting increase in acceptable weight flow. Obviously, research is required regarding diffusion and cooling of flows with thick boundary layers before meaningful conclusions can be made concerning this point.

Figure 18 shows, for a typical nozzle, the maximum ratios of open area to total wall area which are required to achieve various suction flow ratios. A linear suction rate has been used in all cases shown; i.e., starting at .4 feet down the nozzle, the suction flow is linearly increased and results in a total suction flow of either 11% or 22% of the throat mass flow. This also results in a nearly linear $\emptyset$, the maximum $\emptyset$ in all cases occurring at the nozzle exit. Physically impossible $\emptyset$'s are indicated for the 22% suction ratio of Mach number 12. This case was used in Figure 16 for comparison purposes, but should not affect the validity of the indicated trends.

VII. CONCLUDING REMARKS

Based on a comparison of the results of theoretical and experimental investigations, it is concluded that this theory predicts the Mach numbers to about 5% and the boundary layer height to about 10% when the theory is applied to liquid-nitrogen cooled low density nozzles. The investigation covered the range of Reynolds numbers from 150/inch to 3000/inch and the range of Mach numbers form 7.5 to 11.

When the theory was used to determine the effects of wall porosity and cooling on the radius of the uniform core, it was found that, for a fixed throat mass flow and fixed Mach number distribution, this radius was virtually unchanged. Since the cooling and wall suction both served to reduce the boundary layer height, this means that the cooling reduced δ^*/δ enough to keep the boundary layer mass flow constant, while the wall suction removed mass flow at a rate that kept constant the sum of the suction mass flow and the boundary layer mass flow. While this showed there was no direct benefit from cooled porous walls, there were important secondary effects. One of these was the precooling of the suction flow, which would allow a higher mass flow (and larger nozzle) for a fixed cryopump size. Another advantage was that the smaller boundary layer meant a physically smaller and more manageable nozzle. Further, the smaller boundary layer might result in diffuser pressure recovery sufficient to allow conventional mechanical pumps to handle a significant fraction of the flow, permitting a larger total mass flow and a larger nozzle. Since these secondary advantages depend upon the overall system, it is concluded that the merits of a cooled porous wall must be decided from an analysis of the complete wind tunnel system.
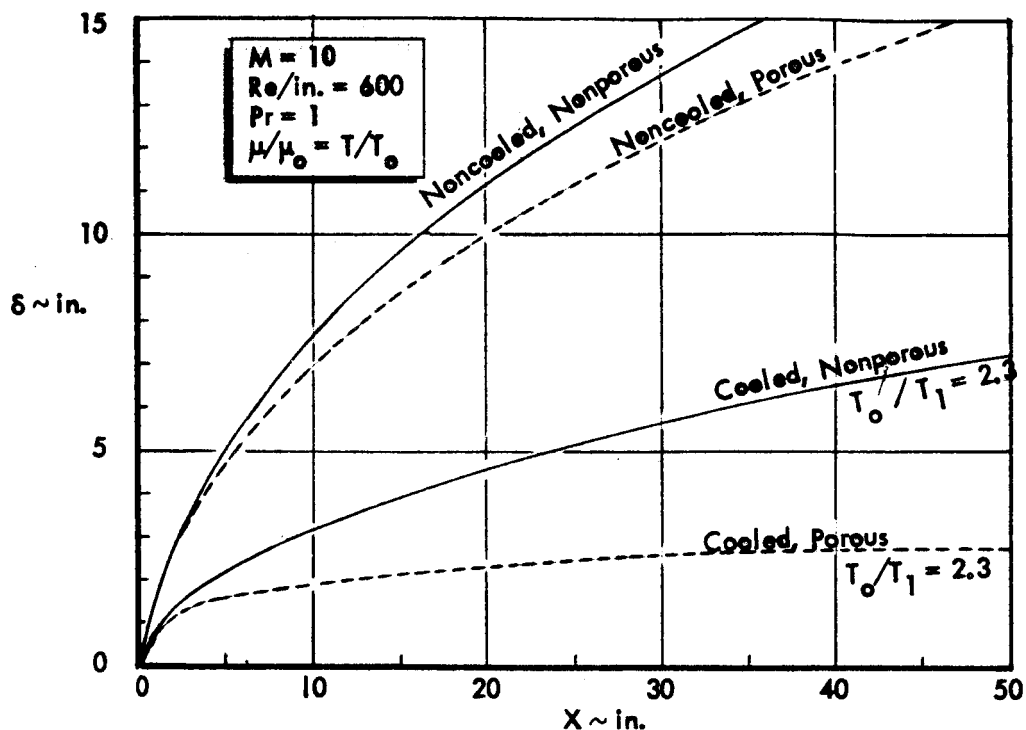
FIGURE 1, EFFECT OF COOLING AND SUCTION ON BOUNDARY LAYER HEIGHT ON A FLAT PLATE.
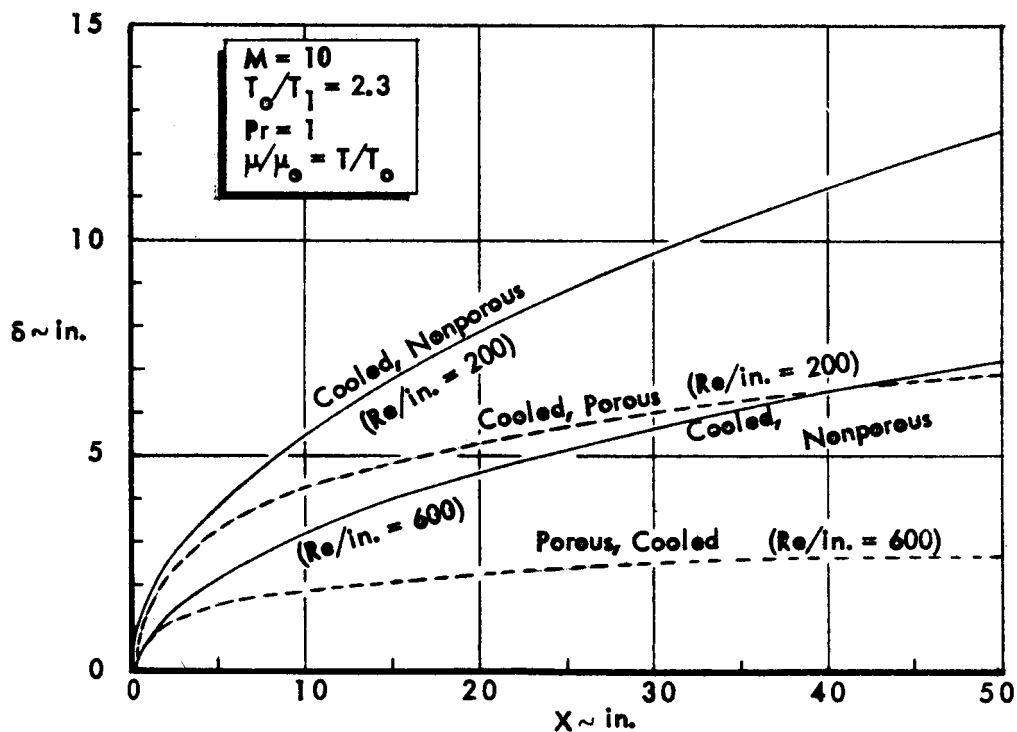

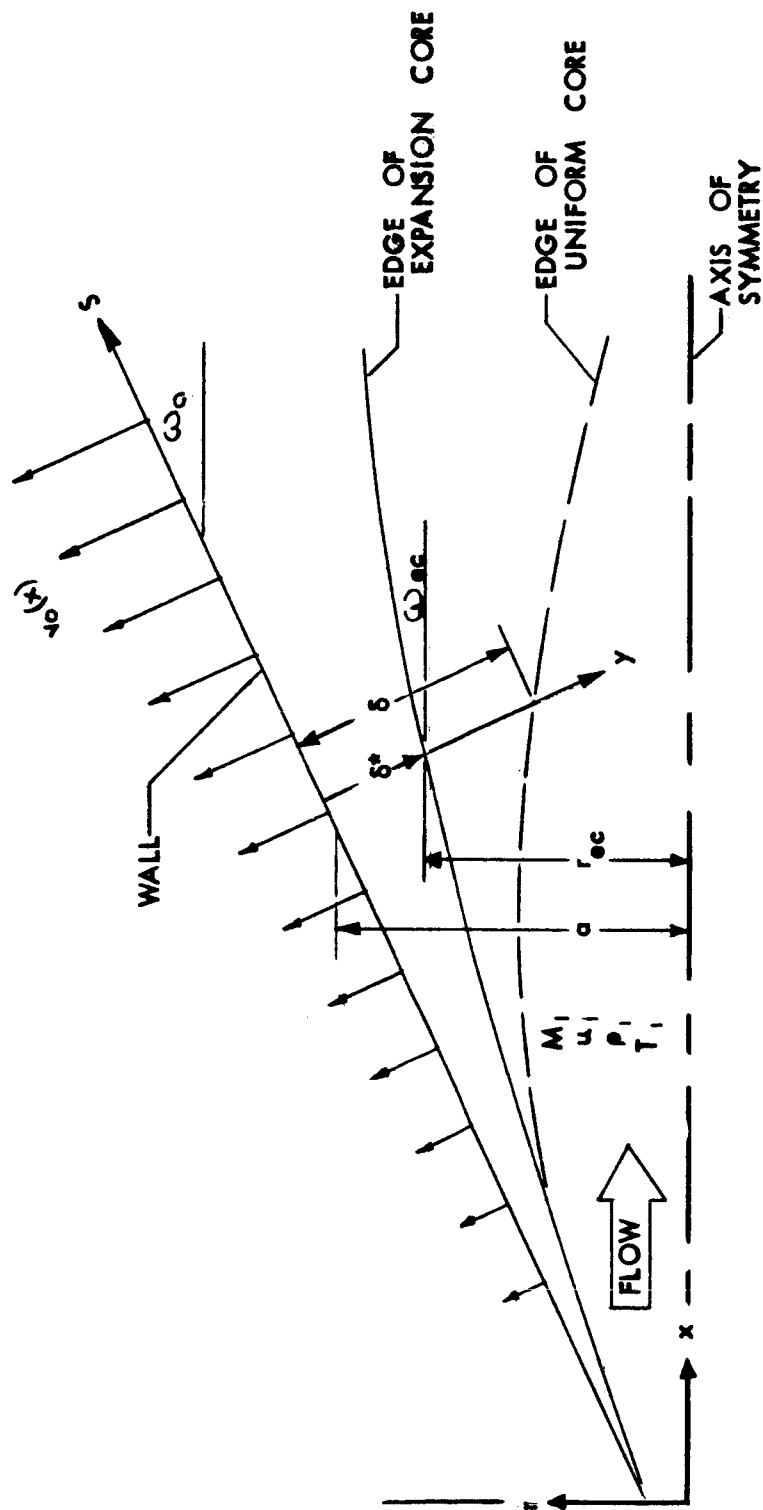FIGURE 2, EFFECT OF UNIT REYNOLDS NUMBER ON BOUNDARY LAYER HEIGHT ON A FLAT PLATE.
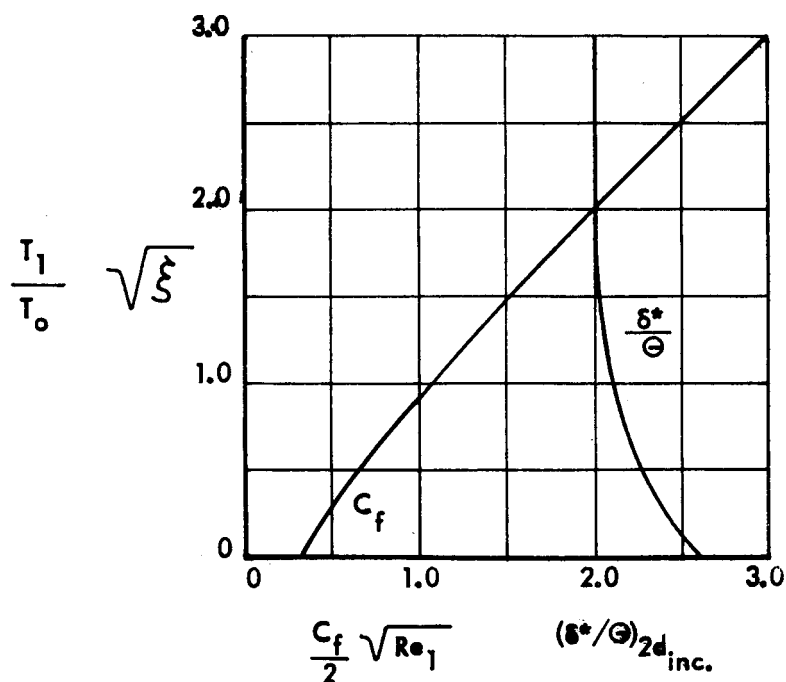
FIGURE 3 , COORDINATE SYSTEM

FIGURE 4. SKIN FRICTION COEFFICIENT AND $(\delta^*/\Theta)_{2d_{inc}}$ FROM
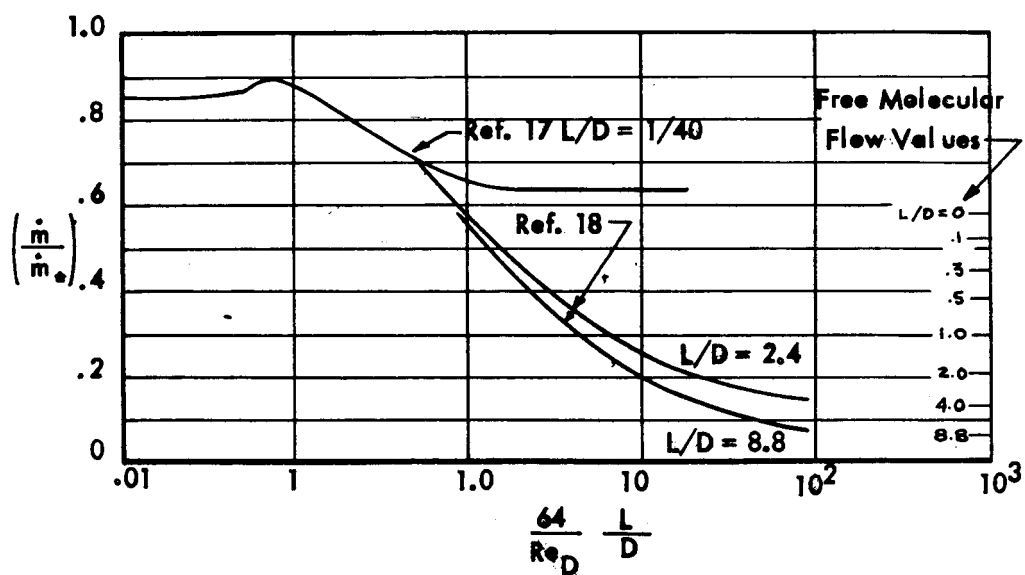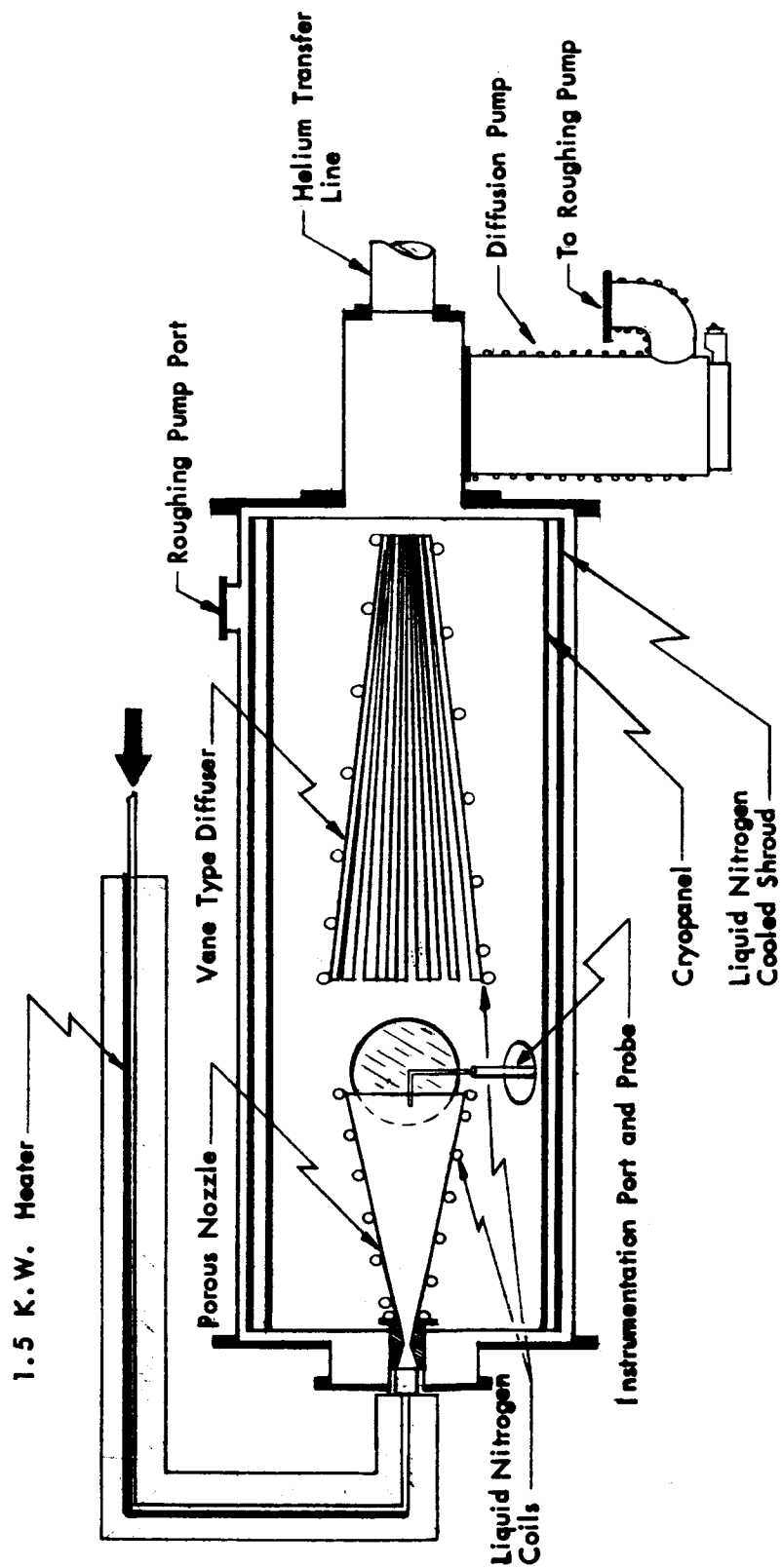
RESULTS OF IGLISCH (REFERENCE 13)

FIGURE 5, EFFECT OF REYNOLDS NUMBER AND TUBE L/D
ON MASS FLOW RATIO

FIGURE 6, EXPERIMENTAL LAYOUT

Helium Transfer Line
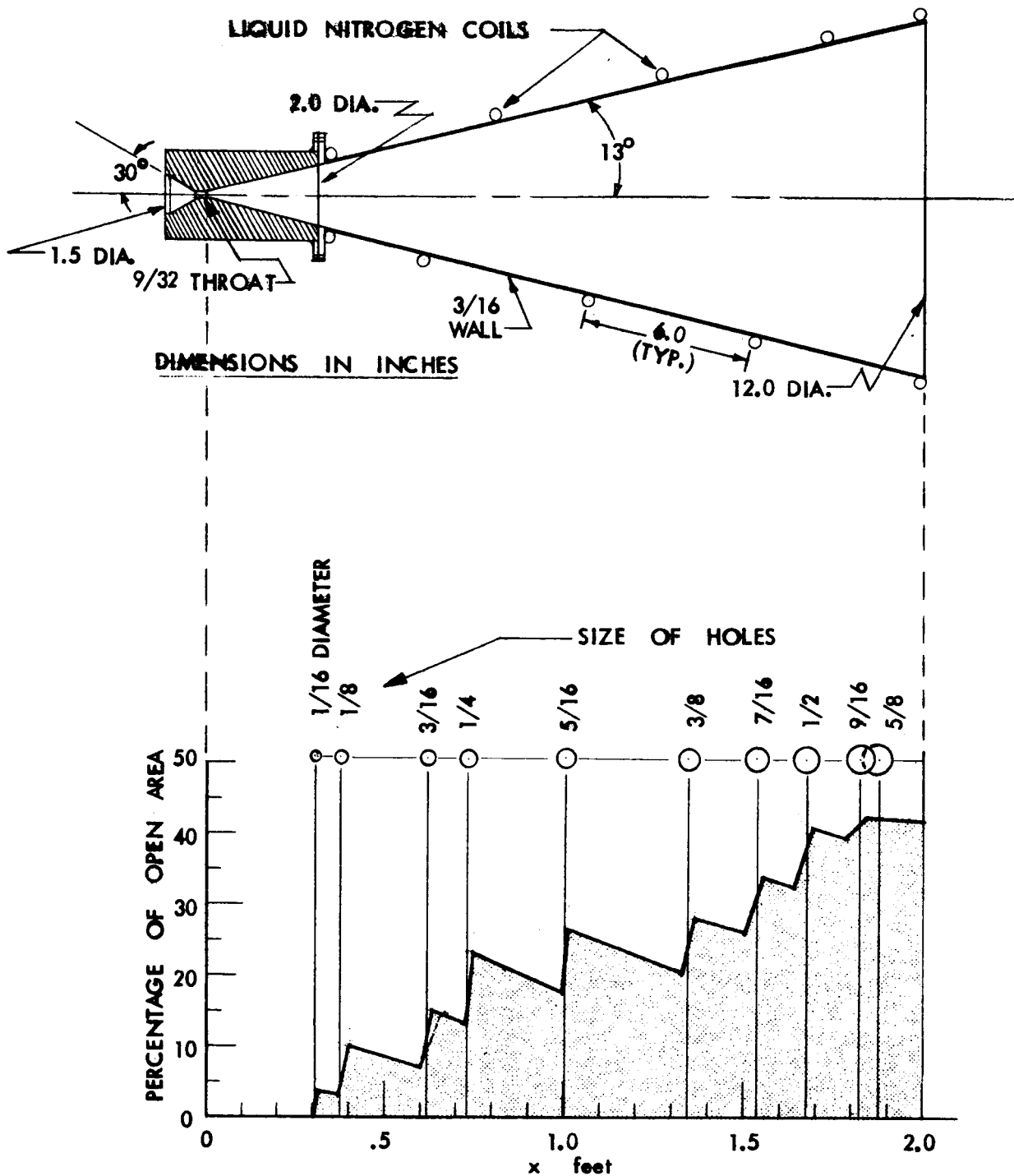
Diffusion Pump

To Roughing Pump

Roughing Pump Port

Vane Type Diffuser

1.5 K.W. Heater

Porous Nozzle

Liquid Nitrogen Coils

Instrumentation Port and Probe

Cryopanel

Liquid Nitrogen Cooled Shroud

Scale: $\frac{1}{18}$

35

FIGURE 7, NOZZLE SCHEMATIC AND
POROSITY DISTRIBUTION

$$\left(\frac{P_{T_M}'}{P_T'}\right)$$
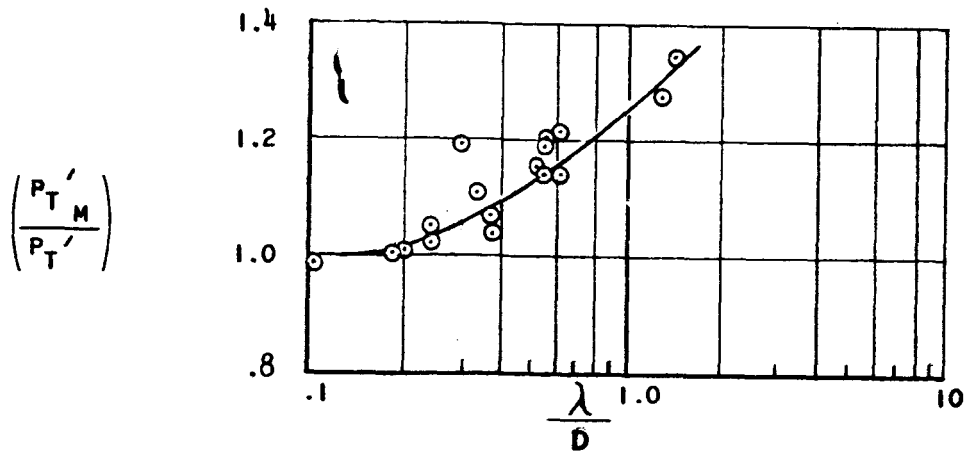
FIGURE 8, EFFECT OF KNUDSEN NUMBER ON
MEASURED PITOT PRESSURE.

SYM	$P_{T_i} \sim$ PSI	$T_{T_i} \sim °R$	$R_e \sim 1/$ IN.
⊙	.10	580	95
▽	.25	780	145
▣	.50	1060	155
▤	.50	520	380
◇	1.00	1210	200
◁	1.45	1260	260
▥	1.95	1300	315
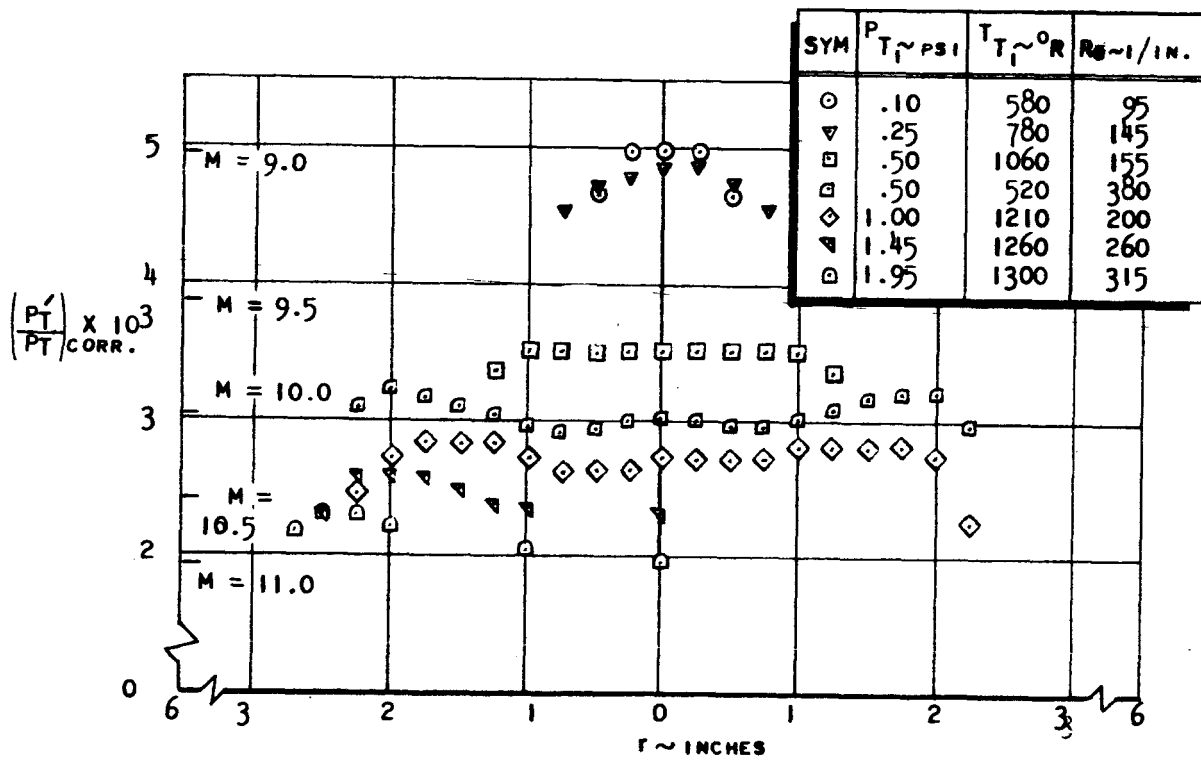
FIG. 9, VARIATION OF PITOT PRESSURE DISTRIBUTION
WITH REYNOLDS NUMBER.

37

Sym	ω	M	Ref
□	13°	8.5 - 11.0	Pres.
⊙	10°	7.5 - 9.0	8
◇	20°	8.5	21
△	17°	10.0	9
▷	20°	4.5 - 5.0	22
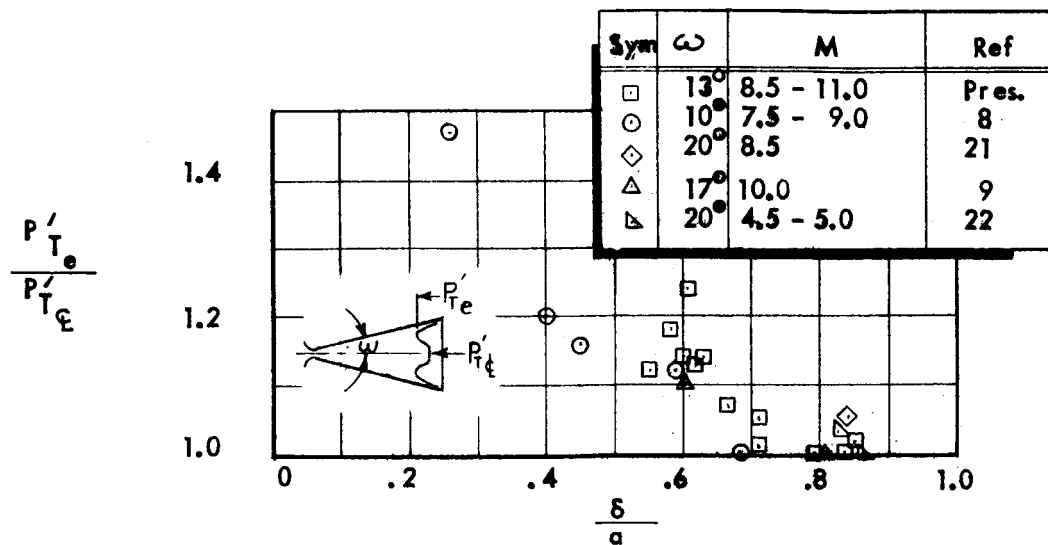
FIGURE 10, VARIATION OF PITOT PRESSURE RATIO WITH $(\frac{\delta}{a})$

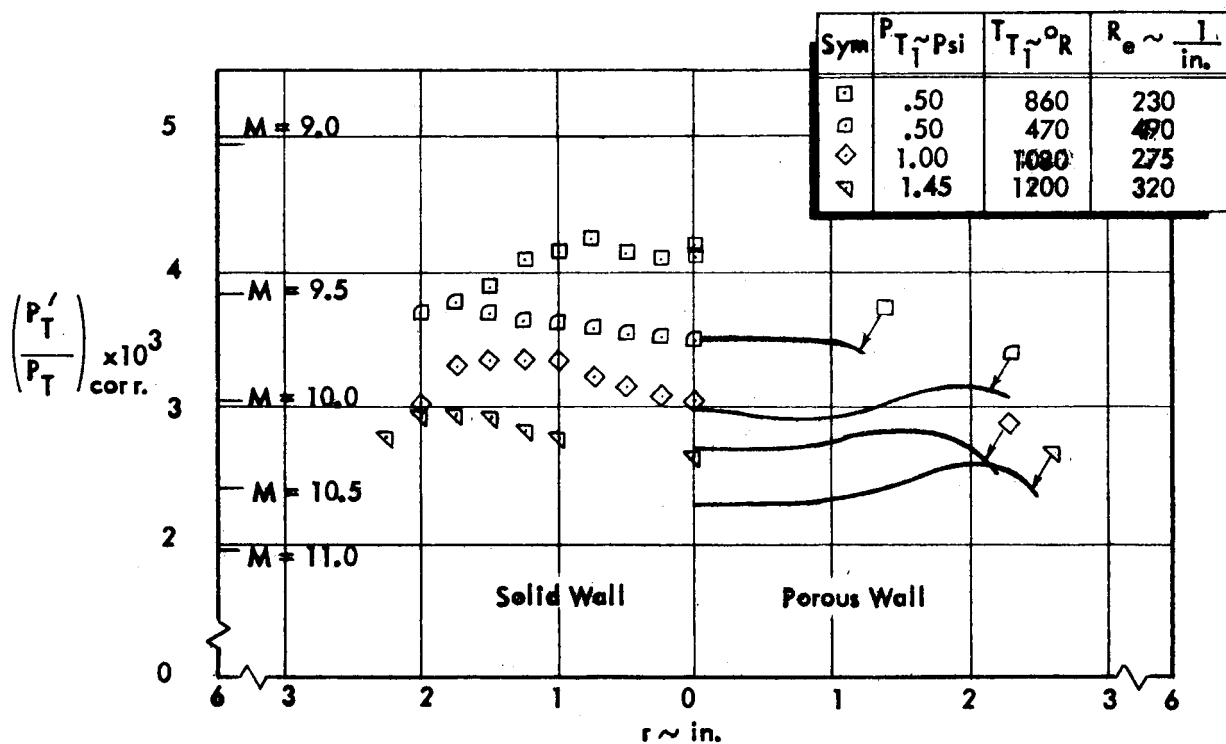| Sym	$P_{T_i} \sim Psi$	$T_{T_i} \sim °R$	$R_e \sim \frac{1}{in.}$
□	.50	860	230
□	.50	470	490
◇	1.00	1080	275
▽	1.45	1200	320

FIGURE 11, COMPARISON OF PITOT PRESSURE DISTRIBUTION,
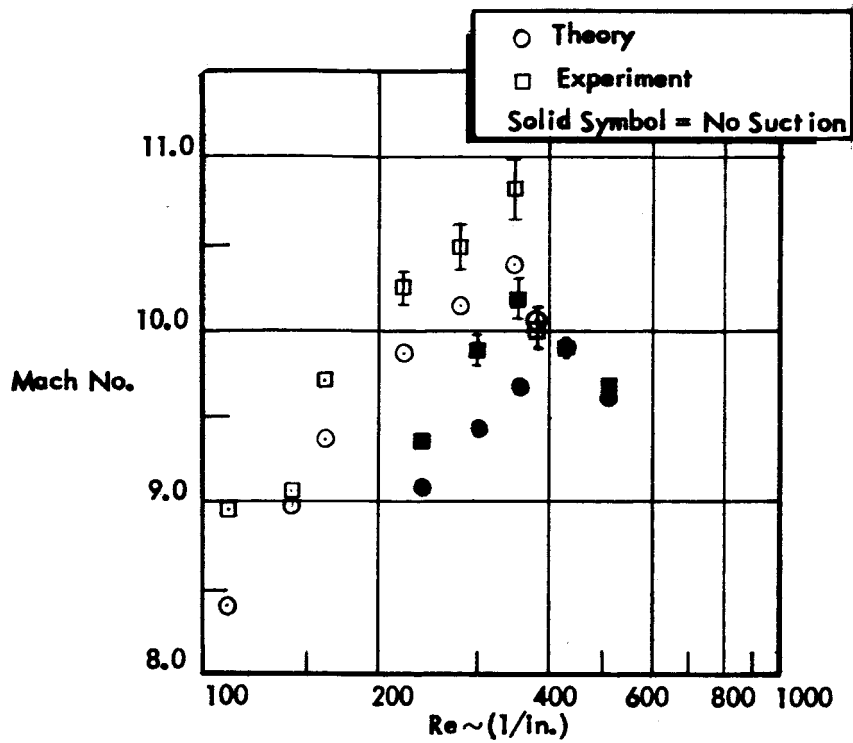SOLID WALL AND POROUS WALL

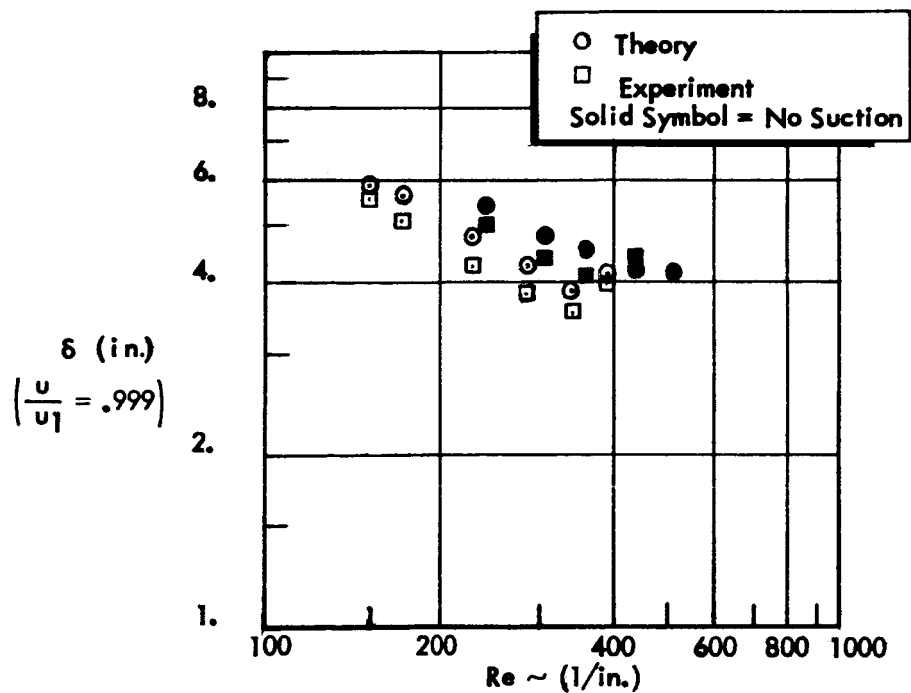FIGURE 12, COMPARISON OF THEORETICAL AND EXPERIMENTAL MACH NO.

FIGURE 13, COMPARISON OF THEORETICAL AND EXPERIMENTAL
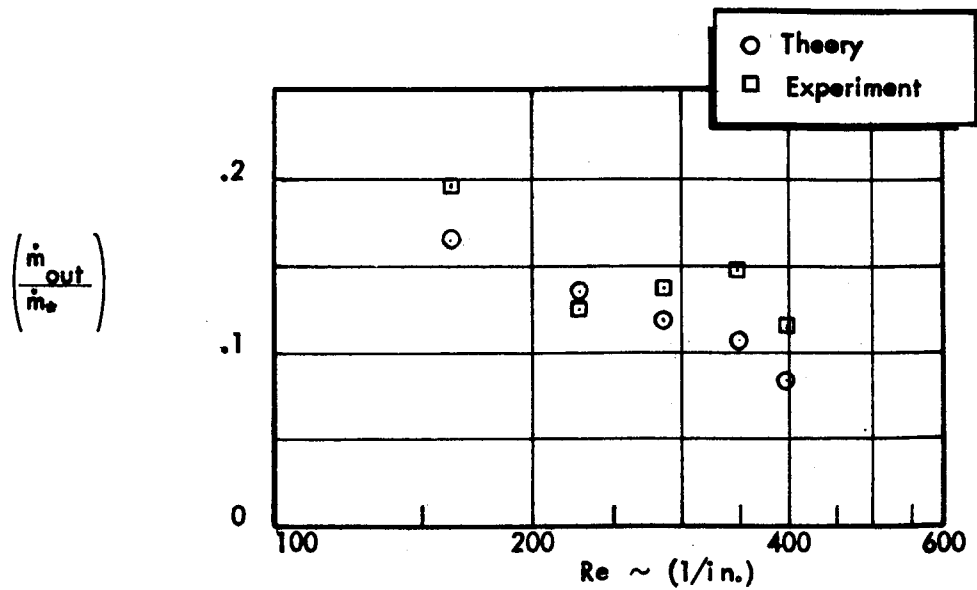BOUNDARY LAYER HEIGHT

FIGURE 14, COMPARISON OF THEORETICAL AND EXPERIMENTAL
SUCTION MASS FLOW
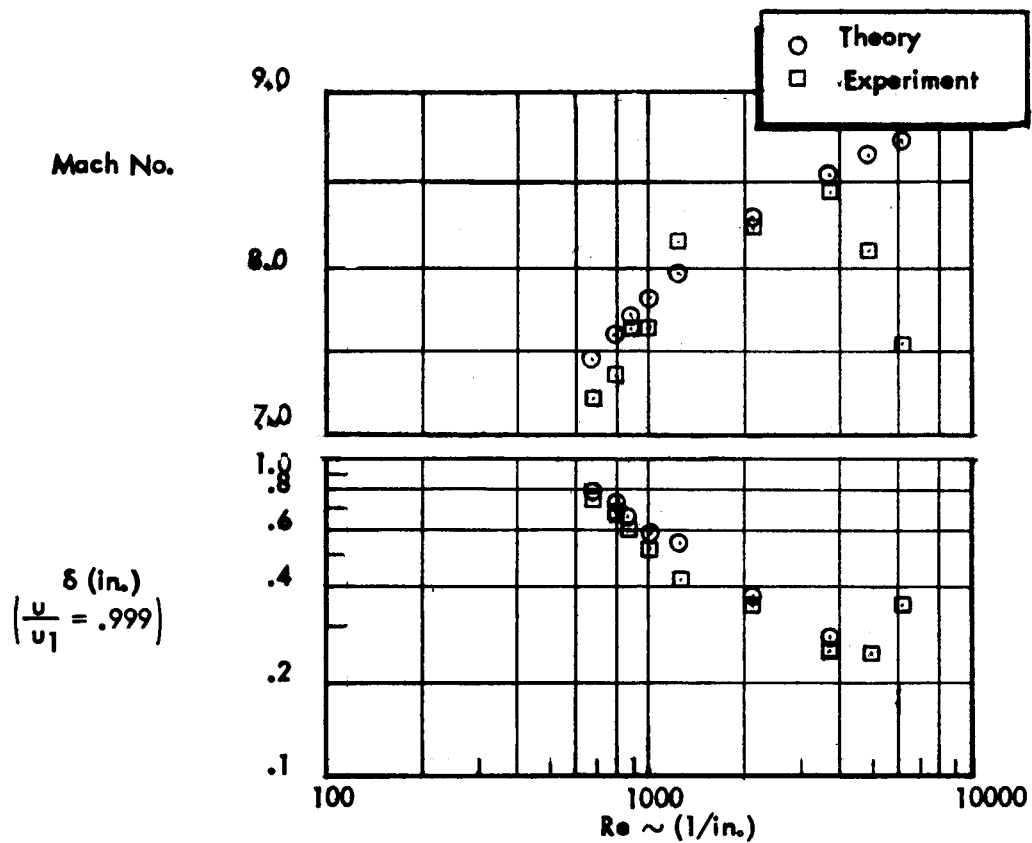
FIGURE 15, COMPARISON WITH EXPERIMENTAL
DATA OF REFERENCE 8

40
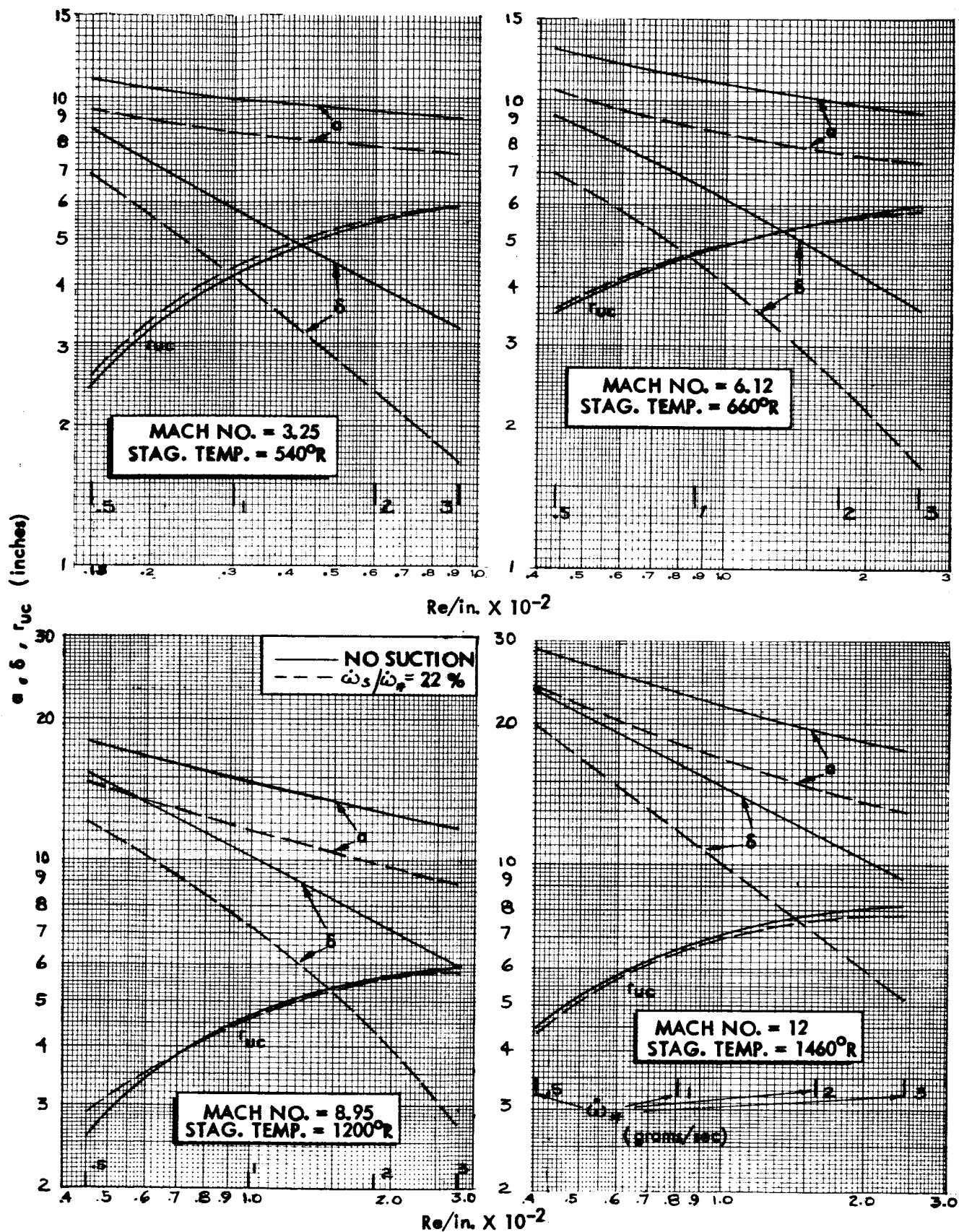
FIGURE 16, EFFECT OF UNIT REYNOLDS NUMBER ON a, δ ,and r_{uc} AT FOUR MACH NUMBERS (Nozzle Length = 4 feet , Wall Temperature = 180°R)

MACH   NUMBER :   12
NOZZLE   LENGTH : 4 FEET
THROAT   RADIUS : .0234 FT.
Re / in. :   800
$\dot{w}_*$: 10 grams / sec
STAGNATION TEMPERATURE : 1460°R
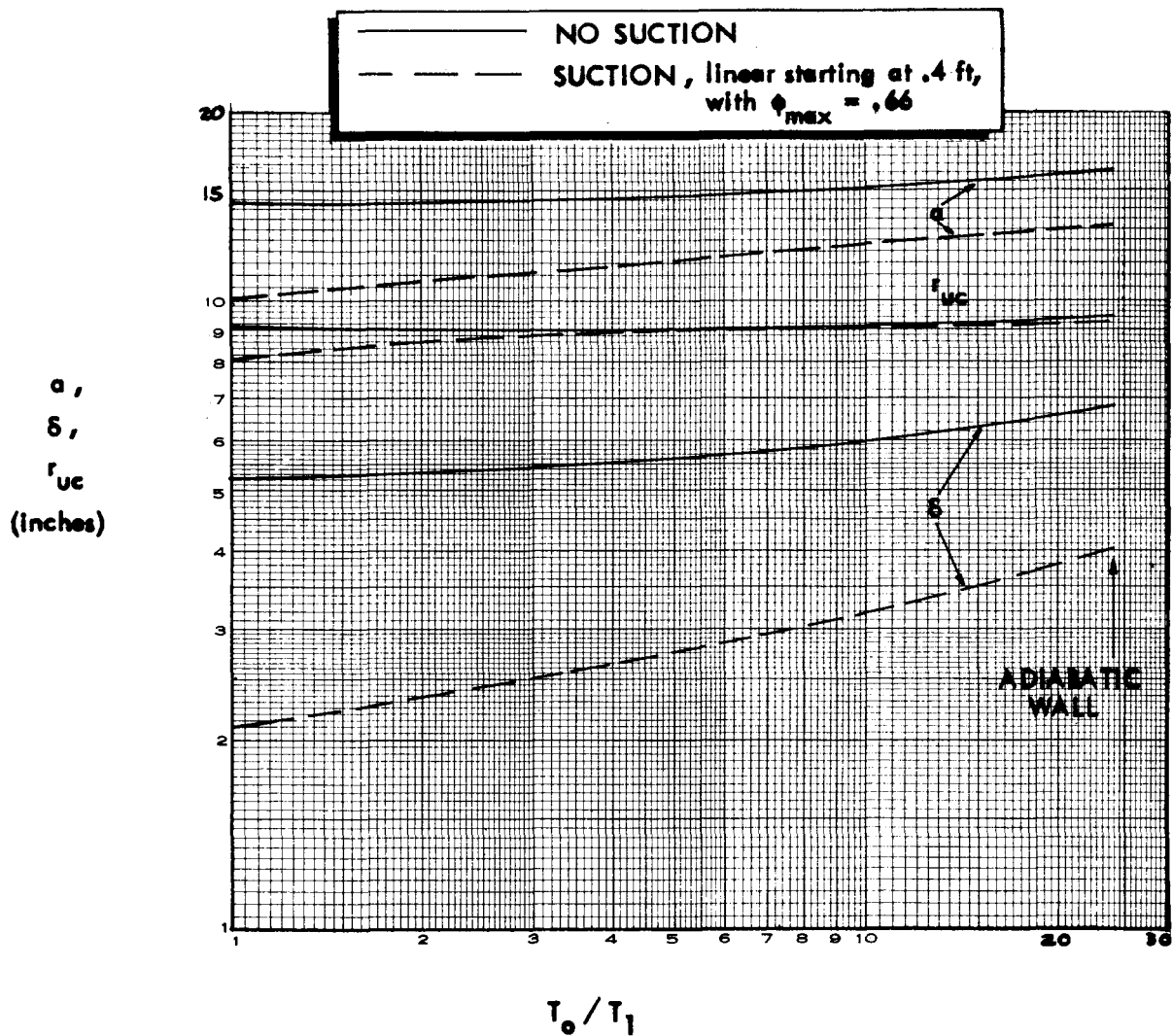
FIGURE 17, EFFECT OF RATIO OF WALL TEMPERATURE
TO FREE STREAM TEMPERATURE ON a , δ , and r_{uc}

CONDITIONS:

NOZZLE LENGTH = 4 FEET
LINEAR Ø STARTING AT .4 FT.
M=12, T_{T_1} = 1440°R
M=9, T_{T_1} = 1200°R
M=6, T_{T_1} = 660°R
M=3, T_{T_1} = 540°R
T_0 = 180°R

ϕ_{max}

M = 12

M = 9

M = 12

M = 6

M = 3

Re/in. X 10^{-2}

FIGURE 18, MAXIMUM OPEN AREA / TOTAL AREA REQUIRED
TO GIVE VARIOUS SUCTION FLOW RATES.

TABLE I

MACH NUMBER DISTRIBUTIONS FOR FOUR-FOOT NOZZLES

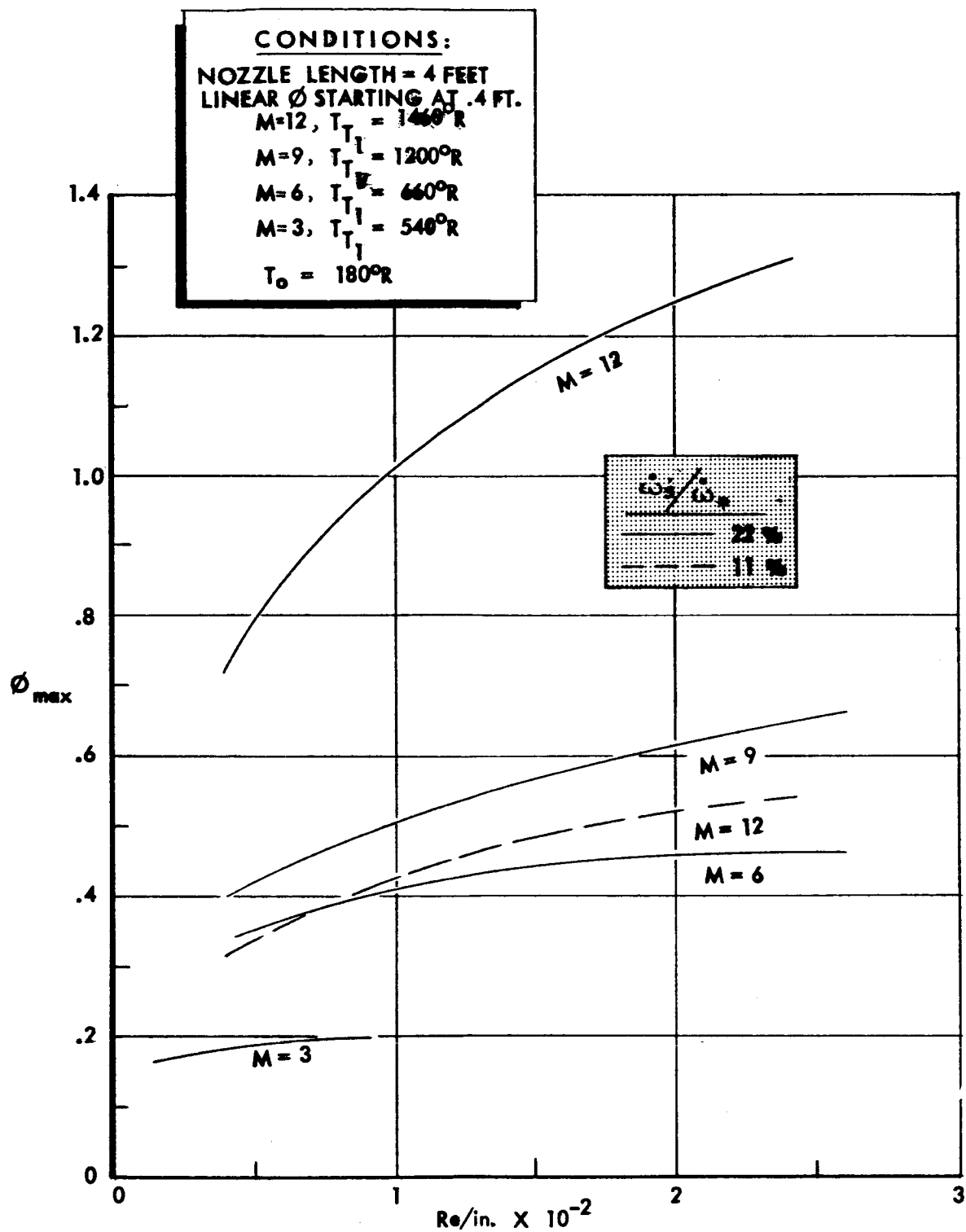| X (feet)	MACH NUMBER			
.2	1.43	2.21	3.21	3.77
.4	1.64	2.75	4.13	4.89
.6	1.80	3.16	4.79	5.70
1.0	2.07	3.80	5.75	6.94
1.2	2.18	4.05	6.12	7.45
1.4	2.29	4.28	6.45	7.91
1.6	2.39	4.49	6.74	8.34
1.8	2.48	4.68	7.01	8.73
2.0	2.56	4.85	7.25	9.10
2.2	2.65	5.02	7.48	9.45
2.4	2.72	5.17	7.69	9.78
2.6	2.80	5.31	7.88	10.09
2.8	2.87	5.44	8.06	10.39
3.0	2.94	5.57	8.22	10.67
3.2	3.01	5.69	8.39	10.95
3.4	3.07	5.81	8.54	11.22
3.6	3.14	5.92	8.70	11.47
3.8	3.20	6.02	8.82	11.72
4.0	3.25	6.12	8.95	11.96
Throat Radii (feet)	.284	.08	.0351	.0234

TABLE II

$$\lambda \text{ vs } \left[\frac{\lambda \ (3\lambda + 5)}{\lambda + 1} + 5\ell n \ \frac{\lambda + 1}{2\lambda + 1} \right] \equiv f(\lambda)$$

$-\lambda$	$f(\lambda)$	$-\lambda$	$f(\lambda)$
0	0	.26	.6816
.01	.005598	.27	.7594
.02	.002280	.28	.8446
.03	.005225	.29	.9381
.04	.009464	.30	1.0409
.05	.01507	.31	1.1540
.06	.02213	.32	1.2787
.07	.03072	.33	1.4165
.08	.04094	.34	1.5692
.09	.05290	.35	1.7390
.10	.06669	.36	1.9283
.11	.08244	.37	2.1405
.12	.1003	.38	2.3795
.13	.1204	.39	2.6504
.14	.1428	.40	2.9597
.15	.1678	.41	3.3159
.16	.1956	.42	3.7309
.17	.2262	.43	4.2212
.18	.2601	.44	4.8107
.19	.2974	.45	5.5373
.20	.3384	.46	6.4640
.21	.3834	.47	7.7090
.22	.4327	.48	9.5385
.23	.4867	.49	12.8017
.24	.5458	.499	24.1271
.25	.6106	.4999	35.6081

45

APPENDIX A*

COMPRESSIBLE LAMINAR BOUNDARY LAYER ON A FLAT PLATE WITH UNIFORM SUCTION AND WALL COOLING

Consider the compressible flow over a flat plate having a uniform suction velocity v_O and constant wall temperature T_O.
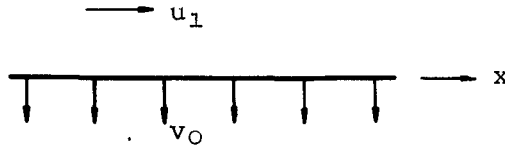
If the suction velocity is small compared to the free stream velocity u, the Prandtl boundary layer equations can be used to describe the flow.

Momentum Equation

$$\rho u \frac{\partial u}{\partial x} + \rho v \frac{\partial u}{\partial y} = \frac{\partial}{\partial y} \left(\mu \frac{\partial u}{\partial y} \right) \tag{1}$$

Continuity Equation

$$\frac{\partial \rho u}{\partial x} + \frac{\partial \rho v}{\partial y} = 0 \tag{2}$$

Energy Equation

If the Prandtl number is assumed to be one, and the wall temperature constant, the energy equation can be replaced by the following relationship:

$$\frac{T}{T_O} = \frac{T_O}{T_1} - \left[\frac{T_1}{T_O} - \left(1 + \frac{\gamma - 1}{2} M_1^2 \right) \right] \frac{u}{u_1} - \frac{\gamma - 1}{2} M_1^2 \left(\frac{u}{u_1} \right)^2 \tag{3}$$

---

* This appendix is a synopsis of the work of Lew and Romano, Reference 6. A prior work by Lew [23] concerning suction on insulated walls greatly facilitates the understanding of Reference 6.

Equation of State

$$p = \rho RT.$$

The continuity equation can be integrated to give

$$\rho v - \rho_0 v_0 = - \int_0^y \frac{\partial}{\partial x} \rho u \, dy. \qquad (4)$$

If this expression is substituted into the momentum equation, the Von Karman momentum integral may be obtained in the form

$$\frac{d}{dx} \int_0^\delta \rho(uu_1 - u^2) \, dy - \rho_0 v_0 u_1 = \mu_0 \left(\frac{\partial u}{\partial y}\right)_0 . \qquad (5)$$

The x and y variables are now transformed as follows: Let

$$dy = L \left[1 + \frac{u}{u_1} \left(\frac{T_1}{T_0} - 1 + \frac{u_1^2}{2 \, cp \, T_0}\right) - \frac{u^2}{2 \, cp \, T_0}\right] dt \qquad (6)$$

and

$$dx = L \, Re \, ds \qquad (7)$$

where L is the plate characteristic length and,

$$Re = \frac{\rho_0 \sqrt{2c_p T_0} \; L}{\mu_0} .$$

Equation (3) can be written in the form

$$\frac{\rho}{\rho_1} = \frac{\gamma - 1}{2} \frac{M^2}{u_1^2} \left\{ 2 \, cp \, T_0 \left[1 + \frac{\bar{u}}{\bar{u}_1} \left(\frac{T_1}{T_0} - 1 + \bar{u}_1^2\right) - u^2 \right]\right\} \qquad (8)$$

where

$$\bar{u} = \frac{u}{\sqrt{2cp\ T_O}} \quad \text{and} \quad \bar{u}_1 = \frac{u_1}{\sqrt{2cp\ T_O}} \quad .$$

Combining equations (6) and (8), we have

$$dy = \frac{L}{2cp\ T_O} \frac{\rho_1}{\rho} \frac{2}{\gamma - 1} \frac{u_1^2}{M_1^2}\ dt = L\ \frac{\rho_1}{\rho} \frac{T_1}{T_O}\ dt. \tag{9}$$

Substituting equations (7) and (9) into (5), and rearranging, one can obtain the transformed momentum integral

$$\frac{d}{ds} \int_{o}^{\delta_t} (\bar{u}\ \bar{u}_1 - \bar{u}^2)\ dt - Re\ \bar{u}_1\ \bar{v}_O = \left(\frac{\partial\bar{u}}{\partial t}\right)_o \tag{10}$$

where δ_t is a measure of the boundary layer thickness and

$$\bar{v}_O = \frac{v_O}{\sqrt{2cp\ T_O}} \quad .$$

Reference 6 suggests both an exponential and a quartic profile for substitution into the integral relationship. However, the quartic profile leads to impossible profile shapes for large Reynolds numbers, and the exponential profile has been selected. The exponential velocity profile is

$$\frac{u}{u_1} = 1 - e^{-\tau}\ (1 - \tau K) \tag{11}$$

where $\tau = t/\delta_t$ and K must be determined by the boundary conditions.

The boundary conditions which the velocity profile must satisfy are

$$\tau \to \infty: \quad \bar{u} \to \bar{u}_1, \quad \frac{\partial\bar{u}}{\partial\tau} \to 0, \quad \frac{\partial^2\bar{u}}{\partial\tau^2} \to 0$$

$$\tau \to 0: \quad \bar{v}_O \left(\frac{\partial\bar{u}}{\partial t}\right)_o = 1/Re\ \left(\frac{\partial^2\bar{u}}{\partial t^2}\right)_o \quad .$$

48

The fourth boundary condition was obtained by evaluating the momentum equation at the wall for the case when μ is proportional to T. (If μ is not assumed proportional to T, the calculations become considerably more complex).

Equation (11) satisfies the first three boundary conditions and the fourth gives

$$K = -\frac{1}{2}\frac{(1 + 2\lambda)}{(1 + \lambda)}$$

where λ has been substituted for the combination of variables

$$\frac{\text{Re } \bar{v}_0 \, \delta_t}{2} \, .$$

Insertion of the velocity profile into the momentum integral relation leads to the differential equation

$$\frac{d\lambda}{ds} = \frac{2R_e \, \bar{v}_0^2}{u_1} \left[\frac{(4\lambda^2 + 4\lambda + 1)\ (1 + \lambda)}{12\lambda^4 + 36\lambda^3 + 37\lambda^2 + 11\lambda}\right] \, . \tag{12}$$

This equation can be solved by integration to yield

$$\xi = \frac{1}{2}\left(\frac{T_0}{T_1}\right)^2 \left[\frac{\lambda(3\lambda + 5)}{\lambda + 1} + 5 \, \ell n \, \frac{(\lambda + 1)}{(2\lambda + 1)}\right] \tag{13}$$

where

$$\xi \equiv \left(\frac{v_0}{u_1}\right)^2 \, \frac{\rho_1 \, u_1 \, x}{\mu_1}$$

and is a known quantity.

Equation (13) thus is used to obtain λ by a trial and error process. Quantities such as C_f or δ, which can be expressed in terms of λ, v_0/u_1, T_1/T_0, and the Reynolds number, can then be determined.

APPENDIX B

SIMILARITY BETWEEN COMPRESSIBLE AND INCOMPRESSIBLE EQUATIONS

Examination of the transformed momentum integral, equation (10) of Appendix A, has shown that it has the same form and boundary conditions as that for incompressible flow with suction. The Karman momentum integral for flat plate flow with Prandtl number of one and having a suction velocity v_0 at the wall is

$$\frac{d}{dx} \int_0^{\delta(\text{or } \infty)} \rho \, (uu_1 - u^2) \, dy - u_1 \rho_0 v_0 = \mu_0 \left(\frac{\partial u}{\partial y}\right)_0 . \tag{1}$$

The boundary conditions which must be satisfied by the velocity profile which is used in equation (1) for incompressible flow are

$$y = 0: \quad u = 0, \quad v_0 \left(\frac{\partial u}{\partial y}\right)_0 = \frac{\mu_0}{\rho_0} \left(\frac{\partial^2 u}{\partial y^2}\right)_0$$

$$\tag{2}$$

$$y \to \infty: \quad u \to u_1, \quad \frac{\partial u}{\partial y} \to 0 \quad \frac{\partial^2 u}{\partial y^2} \to 0.$$

The second boundary condition is obtained by evaluating, at the wall, the momentum equation

$$\rho u \frac{du}{dx} + \rho v \frac{du}{dy} = \frac{\partial}{\partial y} \left(\mu \frac{\partial u}{\partial y}\right).$$

The transformed compressible momentum integral is

$$\frac{d}{ds} \int_0^{\delta_t} (\bar{u} \, \bar{u}_1 - \bar{u}^2) \, dt - \text{Re} \, \bar{u}_1 \, \bar{v}_0 = \left(\frac{\partial \bar{u}}{\partial t}\right)_0 \tag{3}$$

where

t is a normal distance parameter

δ_t is a measure of the boundary layer thickness

$$\bar{u}_1 = \frac{u_1}{\sqrt{2c_p\,T_O}} \qquad \bar{v}_O = \frac{v_O}{\sqrt{2c_p\,T_O}} \qquad ds = L\ Re\ dx$$

$$\bar{u} = \frac{u}{\sqrt{2c_p\,T_O}} \qquad Re = \frac{\rho_O\,\sqrt{2c_p\,T_O}\ L}{\mu_O}$$

L = characteristic length of plate.

Equation (3) may be written as:

$$\rho_O \frac{d}{dx} \int_0^{L\delta_t} (uu_1 - u^2)\ d(Lt) - \rho_O v_O u_1 = \mu_O \left(\frac{\partial u}{\partial(Lt)}\right)_O . \qquad (4)$$

Letting $\psi = Lt$ and the upper limit be ∞, we have

$$\rho_O \frac{d}{dx} \int_0^{\infty} (uu_1 - u^2)\ d\psi - \rho_O u_1 v_O = \mu_O \left(\frac{\partial u}{\partial\psi}\right)_O \qquad (5)$$

This equation has been transformed in y only.

The boundary conditions to be satisfied are

$$\psi = 0: \quad u = 0, \quad v_O \left(\frac{\partial u}{\partial\psi}\right)_O = \frac{\mu_O}{\rho_O} \left(\frac{\partial^2 u}{\partial\psi^2}\right)_O \quad ^*$$

$$\psi \to \infty: \quad u \to u_1, \quad \frac{\partial u}{\partial\psi} \to 0, \quad \frac{\partial^2 u}{\partial\psi^2} \to 0.$$

---

* This boundary condition was derived using the viscosity relation $\mu/\mu_O = T/T_O$. Fortunately, for the wall temperatures of interest in this project (i.e., those near the temperature of liquid nitrogen), this simple relation exactly satisfies the accurate Sutherland relation in the vicinity of the wall. The Sutherland law may be written

(Footnote continued at bottom of next page)

Thus, the momentum integral and boundary conditions have the same forms in the transformed compressible as in the incompressible case. In both cases, the boundary layer form factor δ^*/θ is a function of ξ, the nondimensional distance along the plate, which has previously been defined. Because of the similarity of the y-transformed compressible equations and the incompressible equations, ξ evaluated at the wall is equivalent in the two cases. As shown on page 11 of this report, the incompressible and compressible ξ's are then related by the equation

$$\sqrt{\xi}_{inc} = \frac{T_1}{T_O} \sqrt{\xi} \, .$$

$$\frac{\mu}{\mu_O} = \left[\sqrt{\frac{T}{T_O}} \, \frac{T_O + s}{T + s} \right] \frac{T}{T_O}$$

where s is a constant depending on the gas considered, and the subscript o refers to wall values. The term

$$\sqrt{\frac{T}{T_O}} \left(\frac{T_O + s}{T + s} \right)$$

is of course 1 at the wall, and the rate of change of this term at the wall is

$$\frac{\partial}{\partial y} \left[\sqrt{\frac{T}{T_O}} \left(\frac{T_O + s}{T + s} \right) \right]_O = \left[\frac{1}{2} \frac{T_O + s}{T + s} \frac{1}{\sqrt{T_O \, T}} - \sqrt{\frac{T}{T_O}} \frac{T_O + s}{(T + s)^2} \right]_O \left(\frac{\partial t}{\partial y} \right)_O$$

$$= \left[\frac{T_O}{2T_O^2} - \frac{T_O}{2T_O^2} \right] \left(\frac{\partial T}{\partial y} \right)_O = 0 \qquad \text{for } s = T_O$$

$$= 100°K \text{ for nitrogen.}$$

52

REFERENCES

1. Lee, John D., "Axisymmetric Nozzles for Hypersonic Flows," WADC TN 59-228, The Ohio State University Research Foundation, June 1959.

2. Hurlbut, F. C., and D. E. Beck, "New Studies of Molecular Scattering at the Solid Surface," University of California (Berkely) Technical Report HE 150-166, August 1959.

3. Van Driest, E. R., "Investigation of Laminar Boundary Layer in Compressible Fluids Using the Crocco Method," NACA Technical Note 2597, January 1952.

4. Lew, H. G. and J. B. Fanucci, "On Laminar Compressible Boundary Layer over a Flat Plate with Suction or Injection," Journal of the Aeronautical Sciences, pp. 589-597, Volume 22, Number 9, September 1955.

5. Stalder, J. R., "The Use of Low Density Wind Tunnels in Aerodynamic Research," Rarefied Gas Dynamics, Proceedings of the First International Symposium, held at Nice, Pergamon Press, 1960.

6. Lew, H. G. and F. Romano, "The Compressible Laminar Boundary Layer over a Flat Plate with Uniform Suction and Heat Transfer at the wall," PIBAL Report No. 132, September 1948.

7. Enkenhus, K. R., "The Design, Instrumentation and Operation of the UTIA Low Density Wind Tunnel," UTIA Report No. 44, Institute of Aerophysics, University of Toronto, June 1957.

8. Rogers, Kenneth W., "Preliminary Experiments on a Low Density Hypersonic Wind Tunnel Using a Cooled Proous Nozzle and Diffuser," USCEC Report 65-48, University of Southern California Engineering Center, November 1962.

9. Durand, J. A. and J. L. Potter, "Calculation of Thicknesses of Laminar Boundary Layers in Axisymmetric Nozzles with Low Density, Hypervelocity Flows," AEDC-TN-61-146, December 1961.

10. Johnson, Arlo F., "A Method of Calculating Boundary Layer Thickness in Axisymmetric Nozzles with Laminar Hypersonic Flow," Sandia Corp. Report SC-4370 (RR), October 1959.

11. Maslach, G. J. and F. S. Sherman, "Design and Testing of an Axisymmetric Hypersonic Nozzle for a Low Density Wind Tunnel," WADC-TR-56-341, University of California Report 150-134, August 1956. (AD 97178).

REFERENCES (Cont'd)

12. Probstein, Ronald F. and David Elliott, "The Transverse Curvature Effect in Compressible Axially Symmetric Laminar Boundary Layer Flow," Journal of the Aeronautical Sciences, Volume 23, No. 3, pp. 208-222, March 1956.

13. Iglisch, R., "Exact Calculation of Laminar Boundary Layer in Longitudinal Flow over a Flat Plate with Homogeneous Suction," NACA TM 1205, 1949.

14. Sivells, J. C. and R. G. Payne, "A Method of Calculating Turbulent-Boundary-Layer Growth at Hypersonic Mach Numbers," AEDC-TR-59-3, March 1959.

15. Cohen, Clarence B. and Eli Reshotko, "The Compressible Laminar Boundary Layer with Heat Transfer and Arbitrary Pressure Gradient," NACA-TR-1294, 1956.

16. Loeb, Leonard B., "The Kinetic Theory of Gases," Third Edition, Dover Publications Inc., 1961.

17. Liepmann, H. W., "A Study of Effusive Flow," Reprinted from Aeronautics and Astronautics, GALCIT Publication No. 486, 1960.

18. Brown, DiNardo, Cheng, and Sherwood, "Flows of Gases in Pipes at Low Pressures," Journal of Applied Physics, October 1946.

19. Shapiro, A. H., "Compressible Fluid Flow," Volume 1, The Ronald Press Company, 1953.

20. Cohen, Clarence B. and Eli Reshotko, "Similar Solutions for the Compressible Laminar Boundary Layer with Heat Transfer and Pressure Gradient," NACA-TR-1293, 1956.

21. Chuan, Raymond L., "Research on Rarefied Gasdynamics and Plasmadynamics," USCEC Report 83-101, University of Southern California Engineering Center, September 1962.

22. Kosterin, S. I., N. I. Yschenk, N. T. Belova, and B. D. Kamaev, "Investigation of the Effect of Rarefied Supersonic Flow on the Total Pressure Readings of Impact Probes," Engineering - Physical Journal, Vol. V, Issue 12, December 1962. (Russian).

23. Lew, H. G., "On the Compressible Boundary Layer over a Flat Plate with Uniform Suction," Reissner Anniversary Volume, Contributions to Applied Mechanics, Edited by the Department of Aeronautical Engineering and Applied Mechanics of the Polytechnic Institute of Brooklyn, Published by J. W. Edwards, Ann Arbor, Michigan, 1949.

THEORETICAL AND EXPERIMENTAL INVESTIGATION OF BOUNDARY
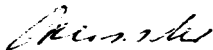LAYER CONTROL IN LOW-DENSITY NOZZLES BY
WALL SUCTION AND COOLING

By

M. R. Bottorff and K. W. Rogers[*]

The information in this report has been reviewed for security
classification. Review of any information concerning Department of
Defense or Atomic Energy Commission programs has been made by the
MSFC Security Classification Officer. This report, in its entirety,
has been determined to be unclassified.
This report has also been reviewd and approved for technical
accuracy.

_____
W. K. Dahm
Chief, Aerodynamics Division

_____
E. D. Geissler
Director, Aero-Astrodynamics Laboratory

_____
[*]Engineering Center, University of Southern California

DISTRIBUTION

INTERNAL

DIR

R-DIR

R-P&VE-DIR

R-QUAL-DIR

R-RP-DIR

R-TEST-DIR

R-AERO
  Dr. Geissler
  Mr. Murphree
  Mr. Dahm
  Mr. Holderer
  Mr. W. W. Vaughan
  Mr. Scoggins
  Mr. Ballance
  Mr. Felk
  Mr. Clark
  Mr. Baur

MS-IP

MS-IPL (8)

MS-H

CC-P

HME-P

EXTERNAL

Ames Research Center
NASA
Moffett Field, California

Manned Spacecraft Center
NASA
Houston 1, Texas

AEDC
Tullahoma, Tenn.

Celestial Research Corporation
1015 Fremont Ave.
South Pasadena, California
Attn: Dr. R. Chum
      M. R. Bottorff
      K. W. Rogers

Scientific and Tech. Info. Facility(25)
Attn: NASA Representative (S-AK/RKT)
P. O. Box 5700
Bethesda, Maryland

Langley Research Center (NASA)
Langley Air Force Base, Virginia

Lewis Research Center
21000 Brookpark Road
Cleveland 35, Ohio

Goddard Space Flight Center (NASA)
Greenbelt, Maryland

Jet Propulsion Laboratory
4800 Oak Grove Drive
Pasadena 3, California